A simple and efficient process for the synthesis of 2D carbon nitrides and related materials

Cora Moreira da Silva, Maxime Vallet, Clement Semion, Thomas Blin, Romuald Saint Martin, Jocelyne Leroy, Diana Dragoe, François Brisset, Cynthia Gilet, Régis Guillot„ et al.

A simple and efficient process for the synthesis of 2D carbon nitrides and related materials.

Cora Moreira Da Silva [1], Maxime Vallet [2], Clément Semion [5], Thomas Blin [1], Romuald Saint-Martin [1], Jocelyne Leroy [3], Diana Dragoé [1], François Brisset [1], Cynthia Gilet [4], Régis Guillot [1], Vincent Huc[1]*.

1: Université Paris-Saclay, Institut de Chimie Moléculaire et des Matériaux d'Orsay (ICMMO), rue du doyen Georges Poitou, FR91405 Orsay, France.

2: Universite Paris-Saclay, Ecole Centrale Sup'Elec, France

3: Commissariat à l'Energie Atomique (CEA), site de Saclay, laboratoire NIMBE, France

4: CNRS-Institut de Biologie Intégrative de la Cellule (I2BC), France

5: Laboratoire d'Etude des Microstructures (LEM, ONERA), Châtillon, France.

Abstract.

This manuscript describes a new process for the synthesis of very high quality 2D Covalent Organic Frameworks (COFs), such a C_2N and CN carbon nitrides. This process relies on the use of a metallic surface as both a reagent and a support for the coupling of small halogenated building blocks. The conditions of the assembly reaction are chosen so as to leave the inorganic salts by-products on the surface, to further confine the assembly reaction on the surface and increase the quality of the 2D layers. We found that under these conditions, the process directly returns few layers material. The structure/quality of these materials is demonstrated by extensive cross-characterisations at different scales, combining optical microscopy, SEM/TEM, EDX, etc... The availability of such very large, high quality layers of these materials opens interesting perspectives, for example in photochemistry and electronics (intrinsic transport properties, high gap substrate for graphene, etc...).

Introduction.

The first preparation of graphene by Geim and Novoselov in 2004 [1,2] sparkled an ever increasing interest in 2D materials. Indeed, along with graphene, dichalcogenides such as MoS_2 or WoS_2 [3, 4], silicene [5, 6], phosphorene [7, 8, 9], hexagonal boron nitride [10, 11] etc… are also being investigated all over the world, due to their fascinating physical [12, 13, 14, 15] and chemical properties [16, 17, 18].
More recently, 2D COFs (Covalent Organic Frameworks), a family of 2D materials obtained by covalent assembly of organic building units have received a growing interest [19, 20, 21, 22, 23, 24].

These compounds are often obtained by surface-confined reaction: a surface acts as a template to promote the adsorption of the reactants, allowing them to organise and condense by means of different bond-forming reactions [25, 26, 27]. A variant of this approach uses the surface both as a template and as a reactant. Many examples of this later approach are to be found in literature, for example by using reactive Cu surfaces in combination with halogenated aromatics [26]. We wish to propose here a new variation of the reactive surface strategy.

We consider here the synthesis of 2D materials from the assembly of soluble, organic building units at the surface of a reactive metal. The solvent used is chosen so as to make the metallic halide by-product insoluble. We reasoned that in such a situation, the presence of this halide by-product would be far from detrimental. Indeed, it could offer a supplementary confinement effect, acting cooperatively with the one associated with the metallic surface. By the same time, the solvent would then provides a continuous supply of reagents to the metal/inorganic salt interface where the reaction takes place. An illustration is shown on Figure 1.

This « double confinement strategy » could improve the quality of synthetic graphene-like 2D materials.

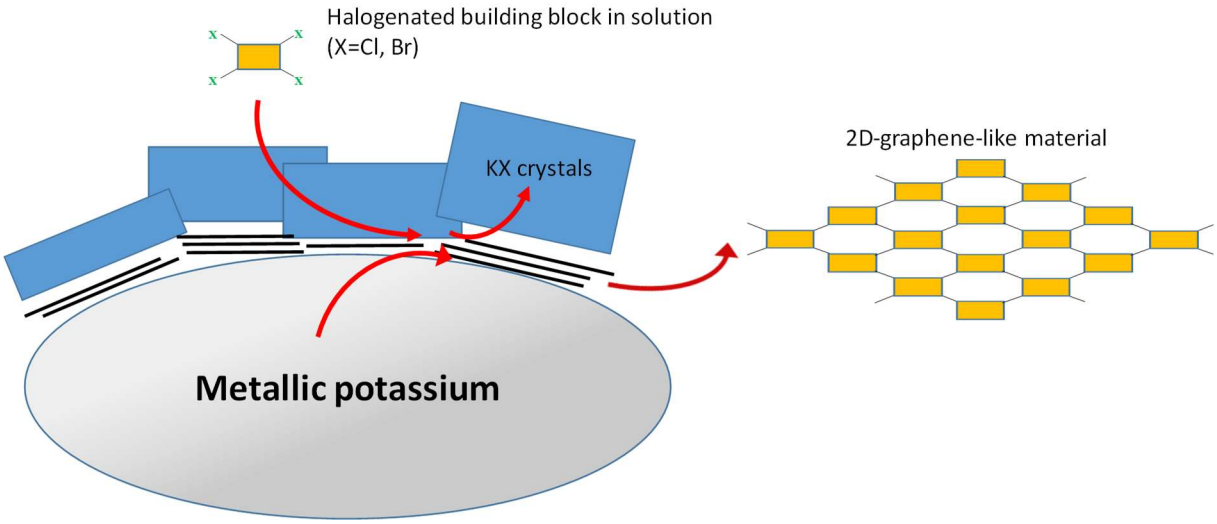

Figure 1: doubly confined growth of 2D materials

Results

Since the pioneering work of Chuanbao et al. [28 29 30], the synthesis of 2D materials by alkali metal-promoted reduction of halogenated precursors was left largely unexplored. Seeking for simple synthesis, that could be performed using common lab equipment, we designed a protocol that runs under close to ambient conditions. To favor a 2D-confined reaction, the solvent used is chosen so as to dissolve the reactant (i.e. allows for the diffusion of the halogenated species to the metallic surface), but neither the final 2D material, nor the inorganic by-products (or any other metal-containing species), to reinforce the confinement effect.

A) : synthesis of CN carbon nitride.

We decided to perform a first experiment targeting a carbon nitride with the general formula CN (Figure 2A) [28, 29, 30, 31 32]. Indeed, carbon nitrides of various stoechiometries are promising for a plethora of applications [33 34 35]. Moreover, the envisioned starting product, cyanuric chloride, is a cheap, commercialy available one.

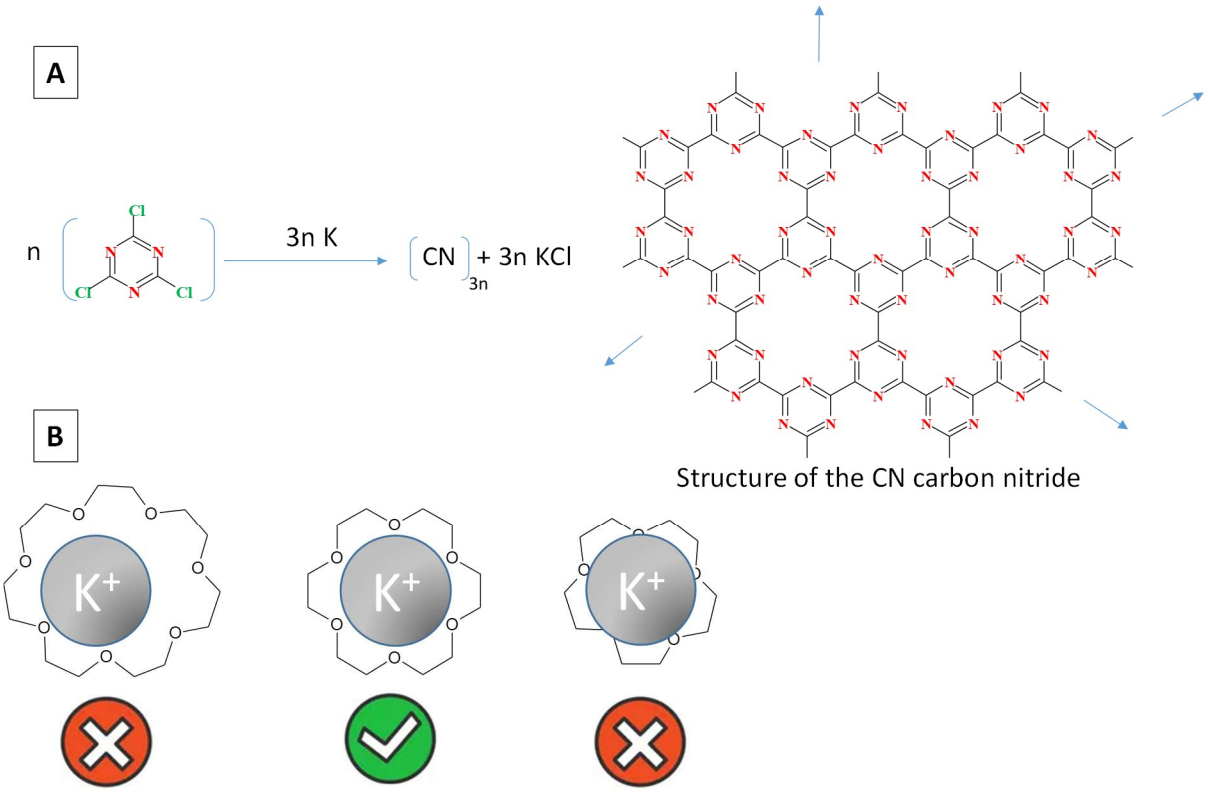

Figure 2: A) synthesis of CN carbon nitride ; B) fit of different macrocyclic cavities with the potassium ion.

Last, potassium was chosen as the reactive metal, because the targeted carbon nitrides do contain coordinating cavities with 6 inward-pointing nitrogen ligands [36]. Indeed, it was shown that K+ ions shows a high affinity for such 6-membered cavities, in comparition with other ones with 5 or 8 coordinating atoms (Figure 2B) [37]. It can thus be guessed that this cation will template the selective formation of six-membered cavities, thus further reinforcing the selectivity towards the formation of the targeted carbon nitrides.

Results.

The details of the synthetic process are to be found in the Supporting Informations (S1), along with a sequence showing the evolution of the reaction media as the reaction goes by (S1A→E).

Crude material analysis

First, an analysis of the crude reaction media (supernatant and solid separately) was performed to qualitatively assess the yield of the reaction.

The amount of remaining organics in the supernantant was found negligible (less than 100 mg). The presence of left residual starting product and/or partial reaction products can thus be considered as rather low.

Then, a sample of the solid obtained after the filtration step (i.e. the removal of soluble residual organics) was directly analysed by XPS spectroscopy (S1H). The Cl 2p spectra can be deconvoluted in two main components, at 197.74 and 199.26 eV. The first one is attributed to KCl (inorganic chloride), and the second one to organic chloride, i.e. to C-bonded chlorine. This later component may be attributed to incompletely reduced species.

The relative surfaces of these two components (along with the very low amount of recovered soluble species) drives to the conclusion that the yield of the reaction is over 80%.

The deconvolution of the N 1s signals shows two components, at 399.21 and 400.57 eV. The 399.21 eV component is attributed to triazinic nitrogens [38, 39, 40, 41]. The higher energy component is attributed to nitrogens bonded to included species, such as metallic cations or H-bonded species. In accordance with the presence of inorganic chloride, strong signals associated with K^+ ions are also observed

Water-washed sample analysis

A final washing with water is necessary, to remove the water-soluble KCl by-product (see SI). CN is obtained as a light brown solid (Figure 3A), easily redispersed in water (Figure 3B).

An optical microscopy analysis of a water suspension shows this material as made of thin, very large flakes (some of them exceeding 500 µm (Figure 3C)). Characteristic features of 2D objects (such as foldings) are clearly observed (Figure 3D). More images are shown in the SI (Figures S1F→G).

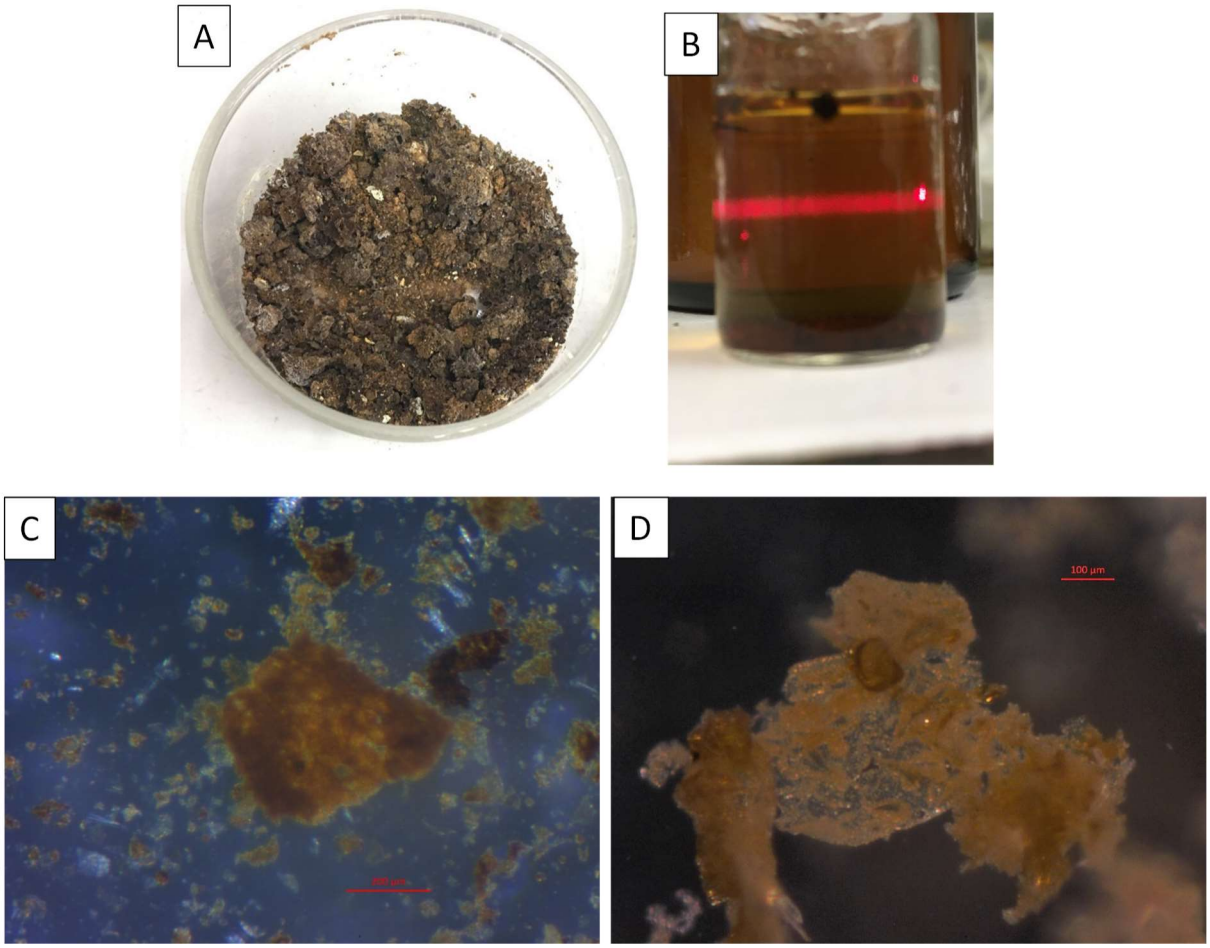

Figure 3. A) the crude CN material; B) water suspended CN, showing the Tyndall effect; C and D) optical microscopy analysis.

Some hollow spheres are also sometimes observed, probably the result of a molding of melted potassium droplets (Figure S1G).

These optical microscopy analyses were also performed using polarised light (Figure 4), with flakes suspended in dispersion oil. Under these conditions, some flakes appear alternatively bright and dark as a function of the relative angles between the polarizer and the sample. This shows that these flakes

are crystalline. The fact that different domains appear inside the flake is attributed to foldings (Figures 4 D and E). Other flakes appear as uniformly bright, regardless of the angle. This could be attributed to the fact that they are constituted of several stacked layers, without orientational correlations between them. The presence of extensive crumpling may also be a plausible explanation, as these foldings may also change the polarisation angle of the transmitted light. A handling experiment of this flake is shown in the SI (Figure S1L) along with one more example of polarised light analysis of a CN flake (S1M).

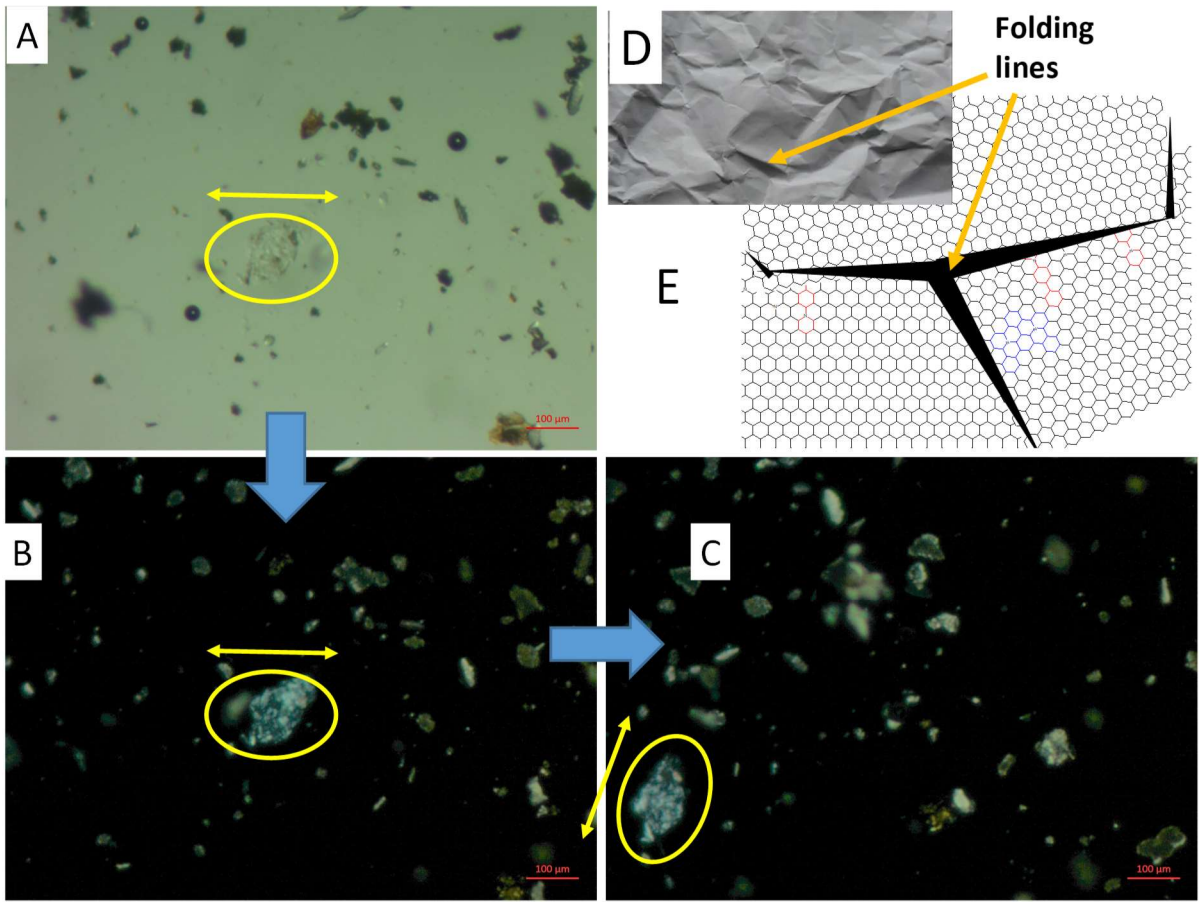

Figure 4: polarized optical microscopy analysis of a CN flake (yellow circle). A) normal light; B) and C) polarised light. The brightness of the flake changes as a function of the angle, evidencing its crystallinity. D) and E): a simple model showing how foldings may give rise to different domains inside a single crystal flake.

SEM/EDS

A SEM microscopy analysis of CN is shown on Figure 5.

Larges flakes (Figure 5A), that tend to roll (Figure 5B) are observed. These features confirm the formation of a layered material.

An EDS analysis (Figure 5C) confirms the presence of the expected elements, along with residual KCl. Oxygen is also observed, probaly as trapped/adsorbed species.

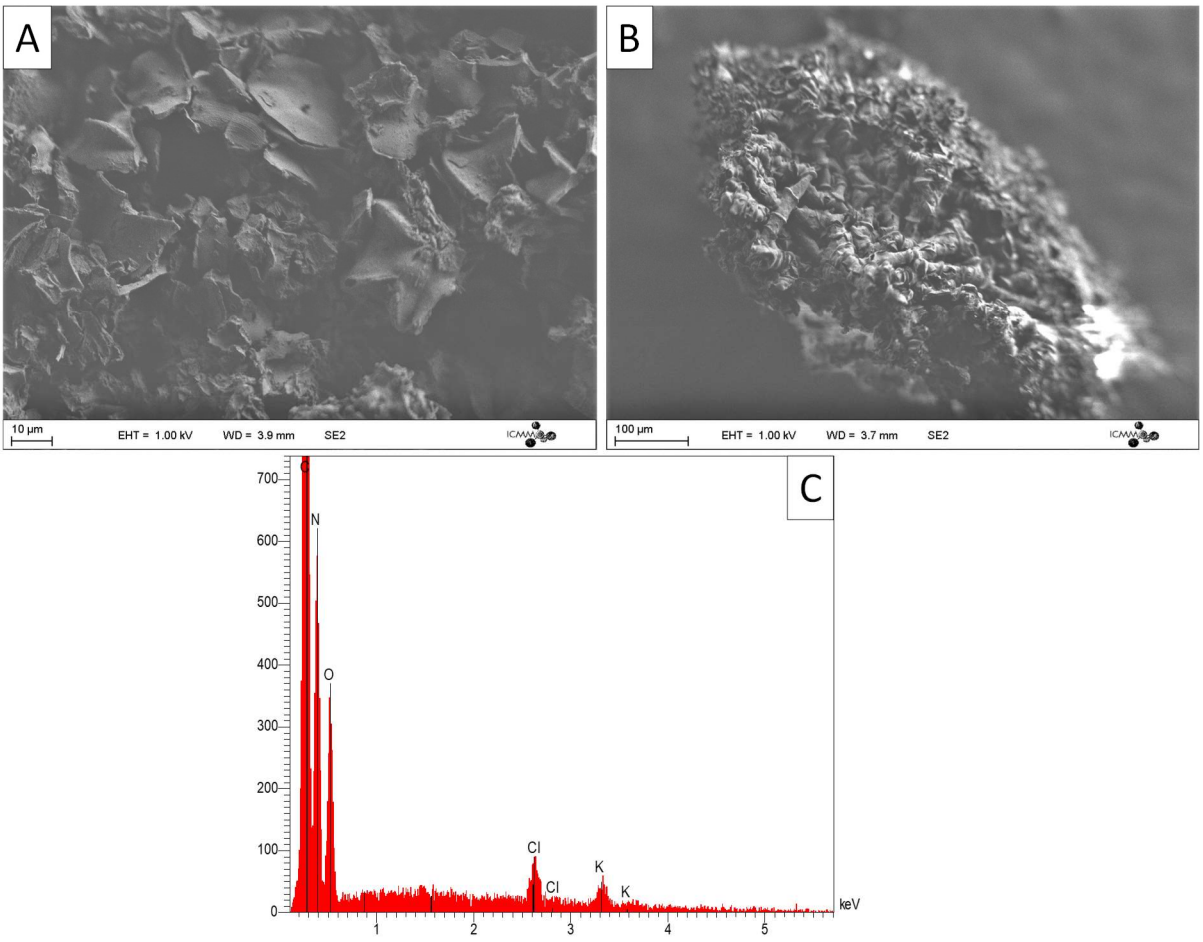

Figure 5. SEM (A and B) and EDS (C) analysis of CN.

XPS

An XPS analysis of a washed sample of CN is shown on Figure 6.

Analysis of the Cl 2p core-level spectrum revealed the presence of two spin-orbit doublets whose Cl $2p_{3/2}$ components are located at 201.3 eV and 198.2 eV. The higher binding energy component is attributed to traces of residual C-Cl bonds while the lower BE component may be related to chloride ions as remaining KCl and $CaCl_2$. Indeed, EDS analyses also confirms the presence of both potassium and calcium (see below, EDS analyses and S1i→J). The very low intensities of the C-Cl signal confirms the low amount of defaults in the material. The deconvolution of C 1s signals shows three main components. The first one at 285eV corresponds to carbon contamination, ubiquitously encountered in such analyses. The two other main components can be attributed to triazinic carbons, from free or N-bonded ones (metallic cations or H-bonded, adsorbed species).

Regarding the N 1s signal, two main components are observed at 399.91 and 401.35 eV [38, 39, 40, 41]. The high energy component, has strongly decreased compared with the crude sample of CN. This confirms the attribution of this high energy peak to nitrogens interacting with included species, such as metallic cations. Oxygen is still observed in the material, showing the presence of a large amount of included, oxygen-containing species. This is coherent with our interpretation of the N 1s signals. Such a tendency to absorb invited species is not surprising, considering the highly porous nature of this material. Similar effects have already been observed with related carbon nitrides [43, 46, 52]. The C/N intensity ratio

between normalized, 1s peaks from the relevant carbon signals and nitrogen is 1.2, close to the expected value of 1.

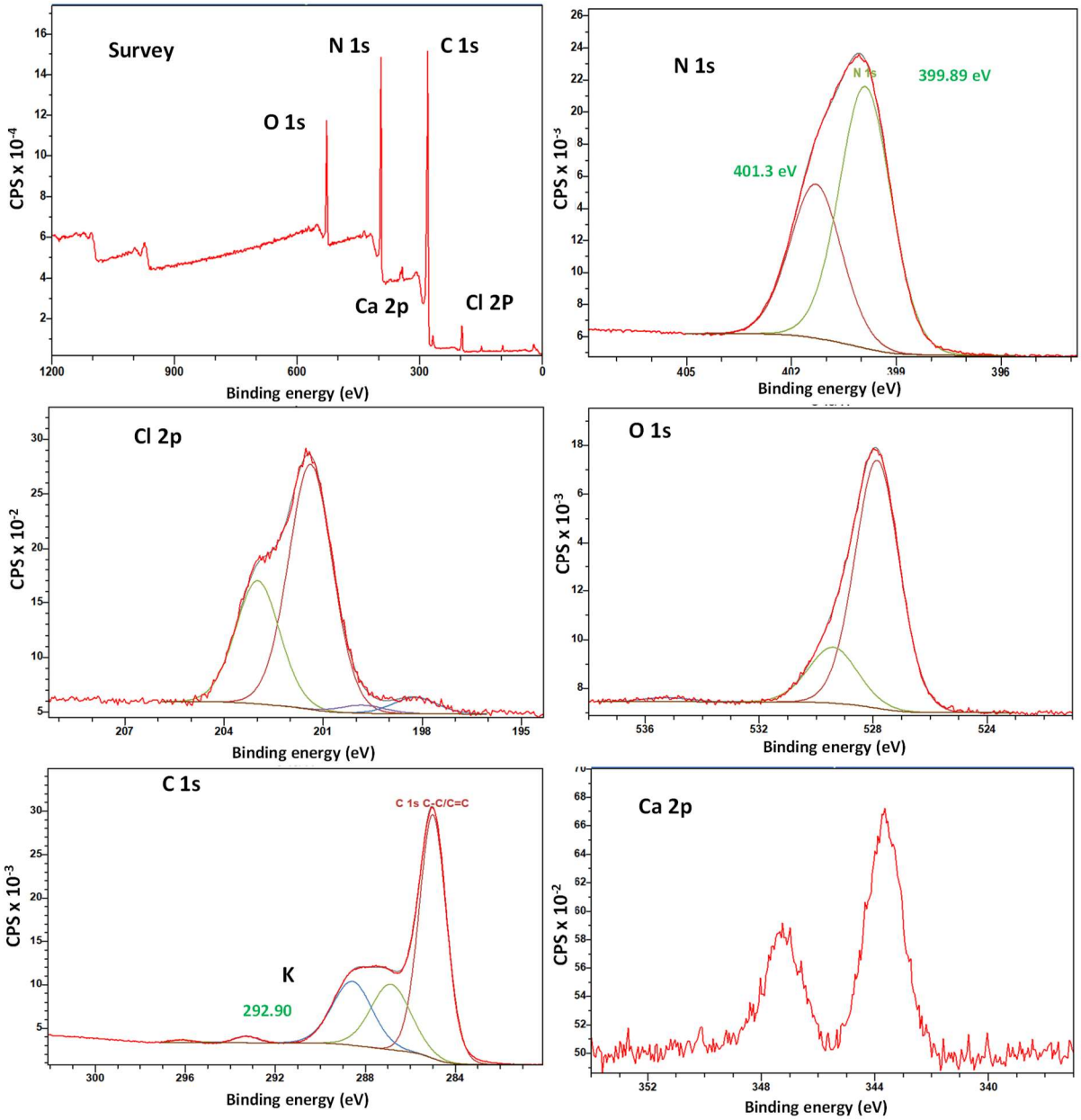

Figure 6. XPS analysis of CN.

XRD

A compared XRD analysis of a crude and washed CN sample was performed. The results are shown on Figure 7.

The crude sample (Figure 7A, red) only shows signals from the by-product of the reaction, i.e. KCl. No others peaks are visible.

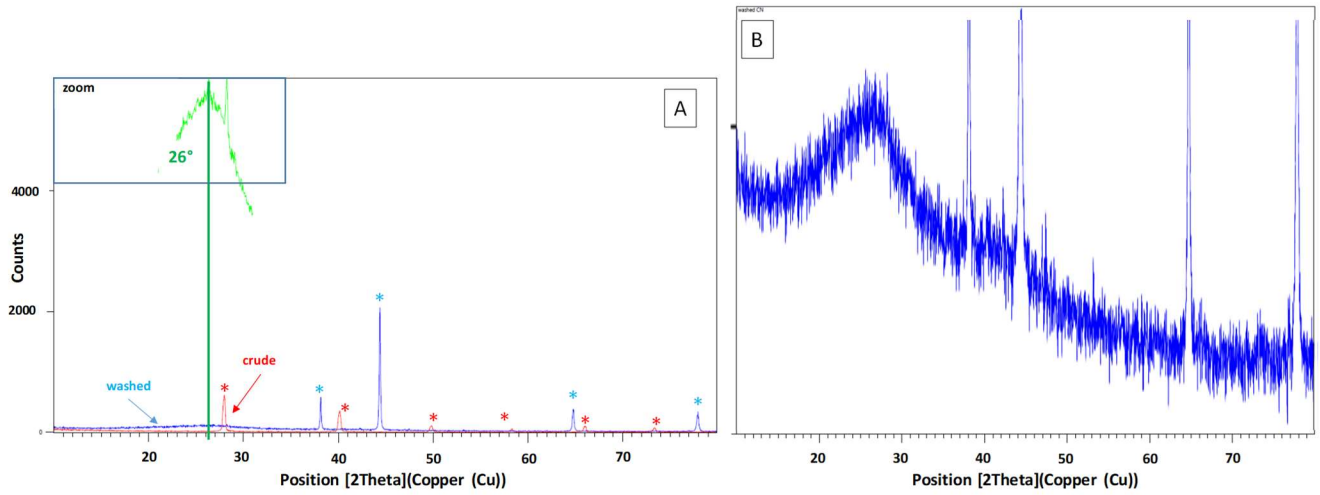

Figure 7: A) compared powder X-ray diffractograms of a crude (red) and washed (blue) CN samples (same batch). Insert (green): zoom over the blue curve. B) Powder X-ray diffractogram of a washed CN sample Blue stars : signals from the aluminum sample holder ; red stars : signals from KCl by-product.

Interestingly, strong evolutions of the same sample are observed upon washing (Figure 7A, blue). Along with the disappearance of the KCl-related signals, a broad peak, centered at 26° appears (Figure 7A, green insert), that was absent from the crude sample. As this peak is characteristic of the interplane spacing of graphenic materials, it can thus be concluded that the flakes mostly exist as individual/few layers objects in the crude material. These flakes are probably kept apart inside a KCl matrix. Upon washing and removal of KCl, these flakes then get aggregated, resulting in the appearence of the 26° peak. Another conclusion that is to be drawn from this comparative study is that the 2D layers are likely to grow as single/few layers agregates during the synthesis.

TEM

The resulting analyses are shown on Figure 8. The images are shown at increasingly high magnifications, to assess the quality of the flakes over different scales.

The material appears as constituted of very large flakes, in accordance with SEM and optical microscopy images. These flakes are very homogeneous and thin, most of them seemingly constituted of bilayers (Figure 8C). They appears quite smooth, with very few visible defects (Figure 8D→F). The well-known affinity of planar, hexacoordinated ligands for uranyl ions was used to load CN with this ion, in order to increase contrasts (Figure S1K-A). TEM analysis of an isolated flake (Figure S1K-B→E) shows the presence of Moiré effects on top of superimposed layers, thus evidencing their crystallinity.

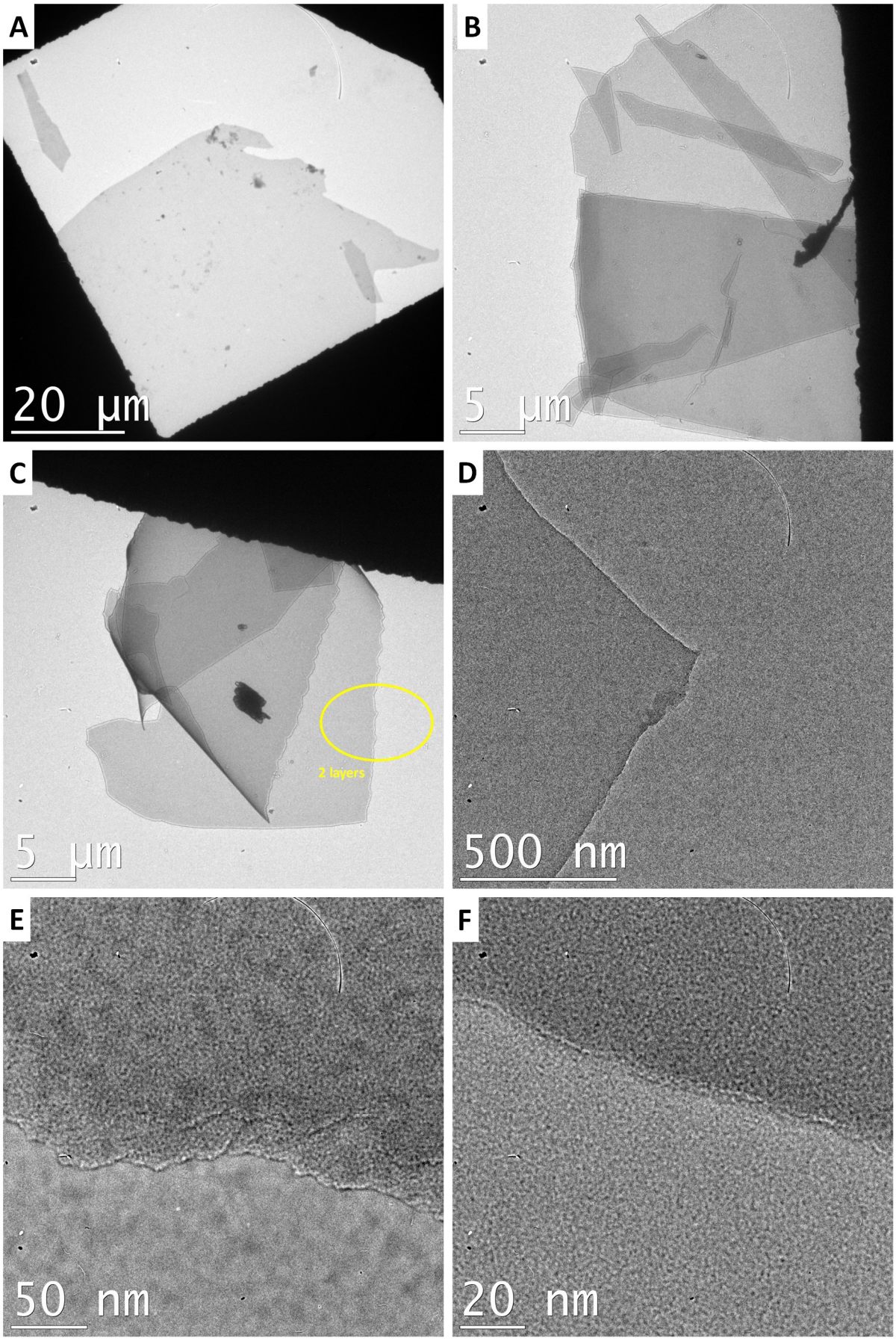

Figure 8. **A→F: TEM images of CN flakes at increasing magnifications.**

EDS

EDS analyses were also performed on this material. Figure 9 shows a detailed analysis at the N-K edge.

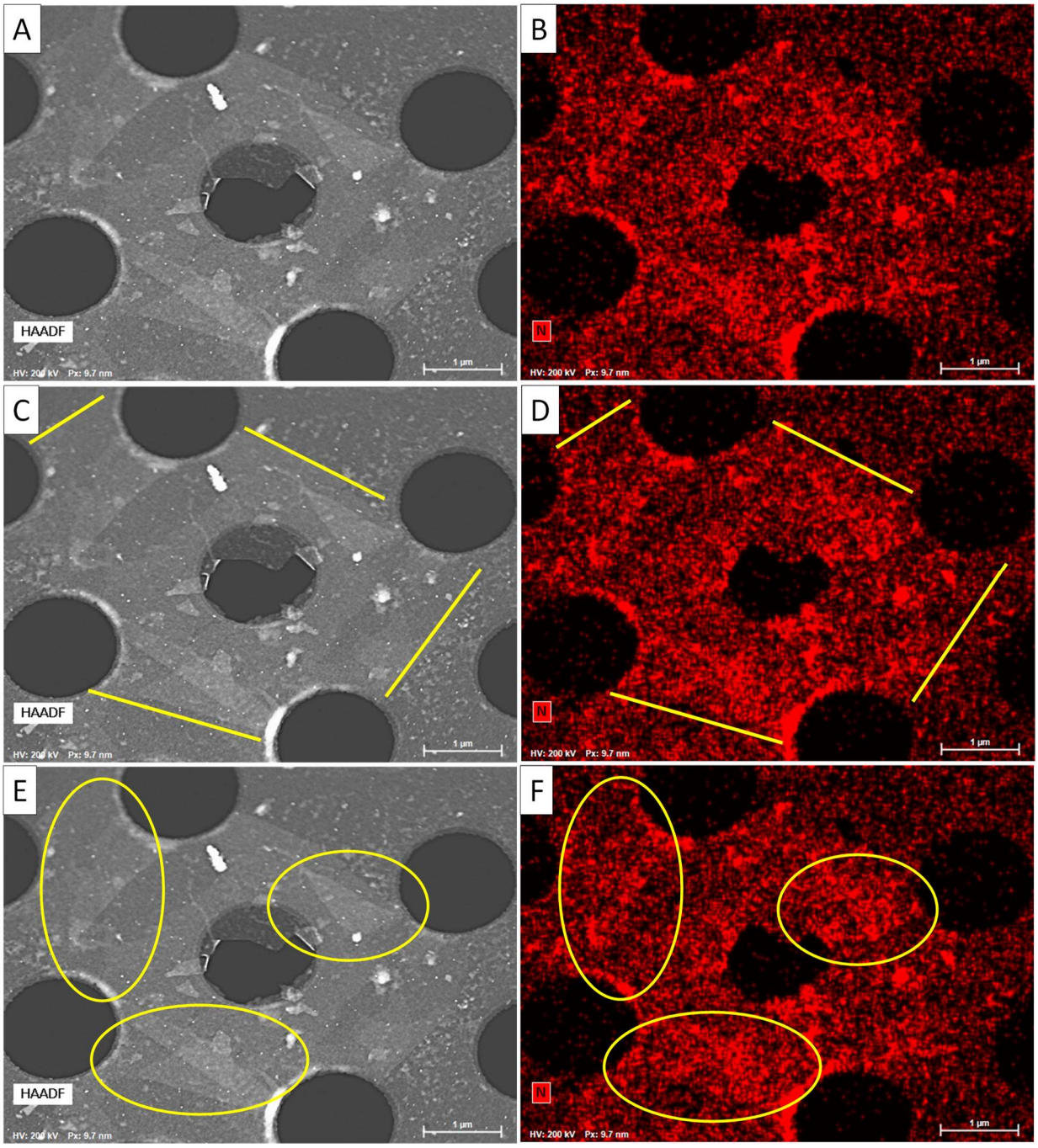

Figure 9. A,B) EDS map of CN at the N-K edge, C→F): highlight of the N-rich areas.

The HAADF micrograph shows the presence of very thin flakes (Figure 9A). A comparison between this image (Figures 9A and 9C) and the corresponding N maping (Figures 9B and 9D) shows a correlation between the shape of the flake and the intensity of the N signal. Moreover, the intensity of this signal increases where thicker flakes are observed (foldings), as evidenced on Figures 9E and 9F (yellow circles). These observations are showing that the flakes are made of a nitrogen-rich material, as expected. This EDS analysis also shows the presence of K and Ca (Figure S1i→J), in accordance with EDS, XPS and EELS (see below) analyses.

EELS

An EELS anaysis of this material (Figure 10) shows the presence of the expected elements C and N. Ca is also observed as an impurity from the starting metallic potassium. The structure of the C 1s and N 1s edges shows a fine structure that is characteristic of extended π-delocalisation [42], in accordance with the expected structure of CN.

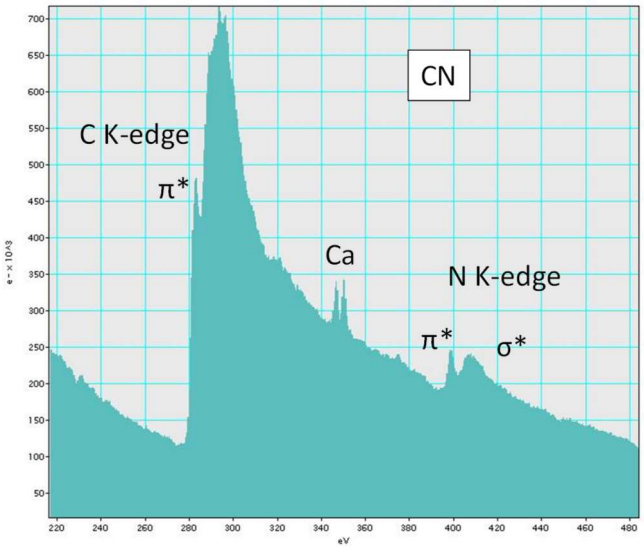

Figure 10. EELS analysis of CN.

All these analyses do show the presence of residual metals (K and Ca) in the material, most probably as cations included inside the coordinating cavities of CN. This may explain the presence of the different signals observed for N 1s by XPS analysis. Ideed, the direct coordination of the N to the positively charged cations probably gives rise to the observed higher energy component.

B) : synthesis of C_2N carbon nitride.

These very encouraging results prompted us to generalise our synthetic strategy. As a second example, we have chosen to synthesise a well documented 2D material, the « C_2N » carbon nitride (Figure 11). Since its discovery in 2015 [43], this material is under the spotlight, due to its tremendous properties in many different fields [44, 45, 46, 47, 48, 49, 50]. Only a handful of synthetic approaches are described so far, all relying on the condensation of complementary carbonyl and amine containing reagents under different conditions [45, 51], or high temperature pyrolysis of organic precursors [52]. In our work, the targeted carbon nitride is obtained by reduction of tetrachloropyrazine using potassium.

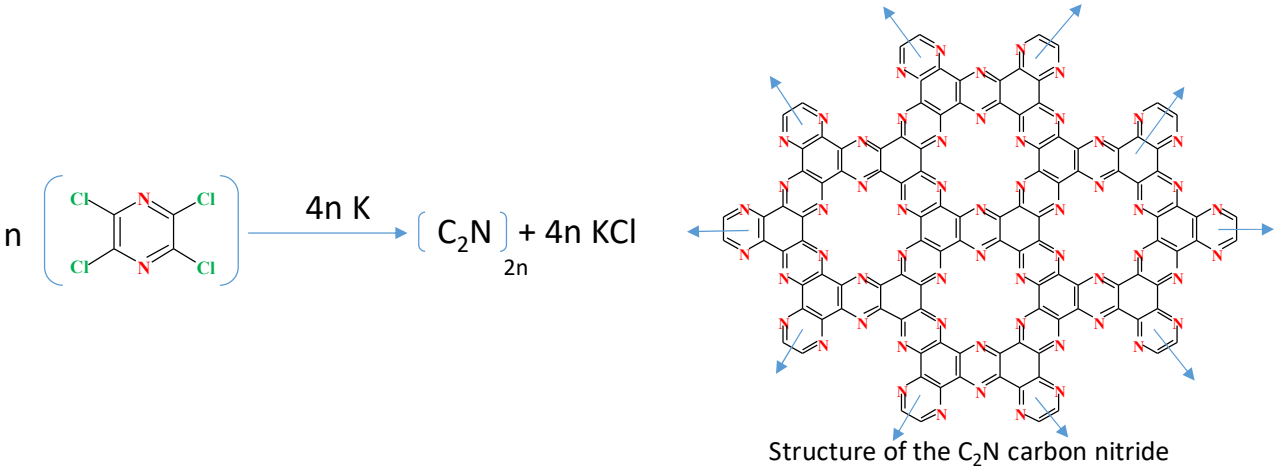

Figure 11. Synthesis of C_2N.

The detailed synthetic procedure is to be found in the Supporting Informations (S2).

Crude material analysis

We first performed an analysis of the crude material, to qualitatively estimate the yield of the synthesis. The reaction media was filtered, and the resulting black solid washed with acetone (see S2A→E). All the organic phases were combined and evaporated to dryness on a vacuum line, leaving a very small amount (50mg) of a dark brown residue. A sample of the solid black material left after filtration was then analysed. An XPS analysis of this crude sample is shown on Figure S2F. It shows the presence of strong potassium signals (Figure S2F-D) as cationic species. Analysis of the corresponding Cl 2p signals (Figure S2F-B) shows the presence of two different kinds of chlorine atoms. The one with the lowest binding energy is characteristic of anionic chlorine, and is thus ascribed to KCl. This is confirmed by the measured 1/1 K/Cl ratio. A second Cl component with a higher binding energy is attributed to organic chlorine (i.e. bonded to carbon atoms). A comparition of the relative areas of these two species (along with the very small amount of soluble material (50mg), see previous paragraph), shows that the yield of the reaction is above 90%.

An analysis of the N 1s signals (Figure S2F-C) reveals two components attributed to pyridinic-type nitrogens [38, 39, 40, 41]. The higher energy one probably belongs to metallic cations-bonded nitrogens. As already mentioned, strong signals of potassium ions (along with a few percent of calcium) are also observed.

Washed sample analysis

The purified C_2N material is obtained as a fluffy, black powder, (Figures 12A and B).

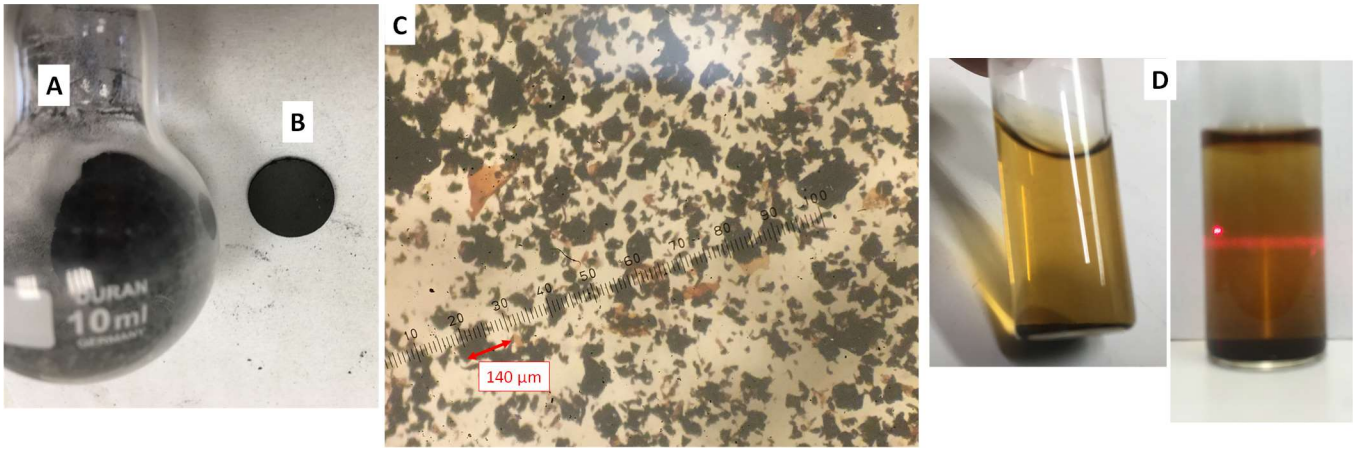

Figure 12: washed C_2N. Optical microscopy (A); (B) same material as a compressed pellet ; C): optical microscopy of an HCl dispersed C_2N sample; D) orange-colored HCl suspension of C_2N showing the Tyndall effect.

An observation of the same material as an acidic (1M HCl) water suspension shows it to be constituted of large, variously aggregated and folded flakes, with sizes ranging from a few tens to 300 µm (Figures 12C and 12D). The color of the thinnest flakes appears as deep orange, rapidly turning to black with increasing thickness (S2j). The bright orange color of acidic C_2N suspensions confirms that a significant amount of the material is made of single/few layers flakes (Figure 12E). In some instances, tubular (S2H) or shell-shaped objects (S2i) were also observed. In the later case, this is likely to be the result of a molding of melted potassium droplets, getting encapsulated during the growth of C_2N around them.

Interestingly, we also found that some flakes (thin enough and not too folded/crumpled) do rotate the polarisation plane of incident polarised light, as expected for single crystals. One example is shown on Figure 13. Other examples are provided in the SI (Figures S2K→S2M). The flakes (after washings) were dried on a glass plate overnight and diluted in dispersion oil to ease their observation and handling.

These extremely thin flakes are nearly invisible (even with the microscope). They can only be detected due to their changing brightness under polarized light. As the flakes gets thicker, the effect disappears, probabaly due to: i) the absence of correlation of the orientation of the layers inside thick flakes, ii) their increasing absorbance and iii) the presence of foldings, that tend to average the effect on polarised light. Note that the observation of single layer graphene using polarised light has already been reported [53, 54].

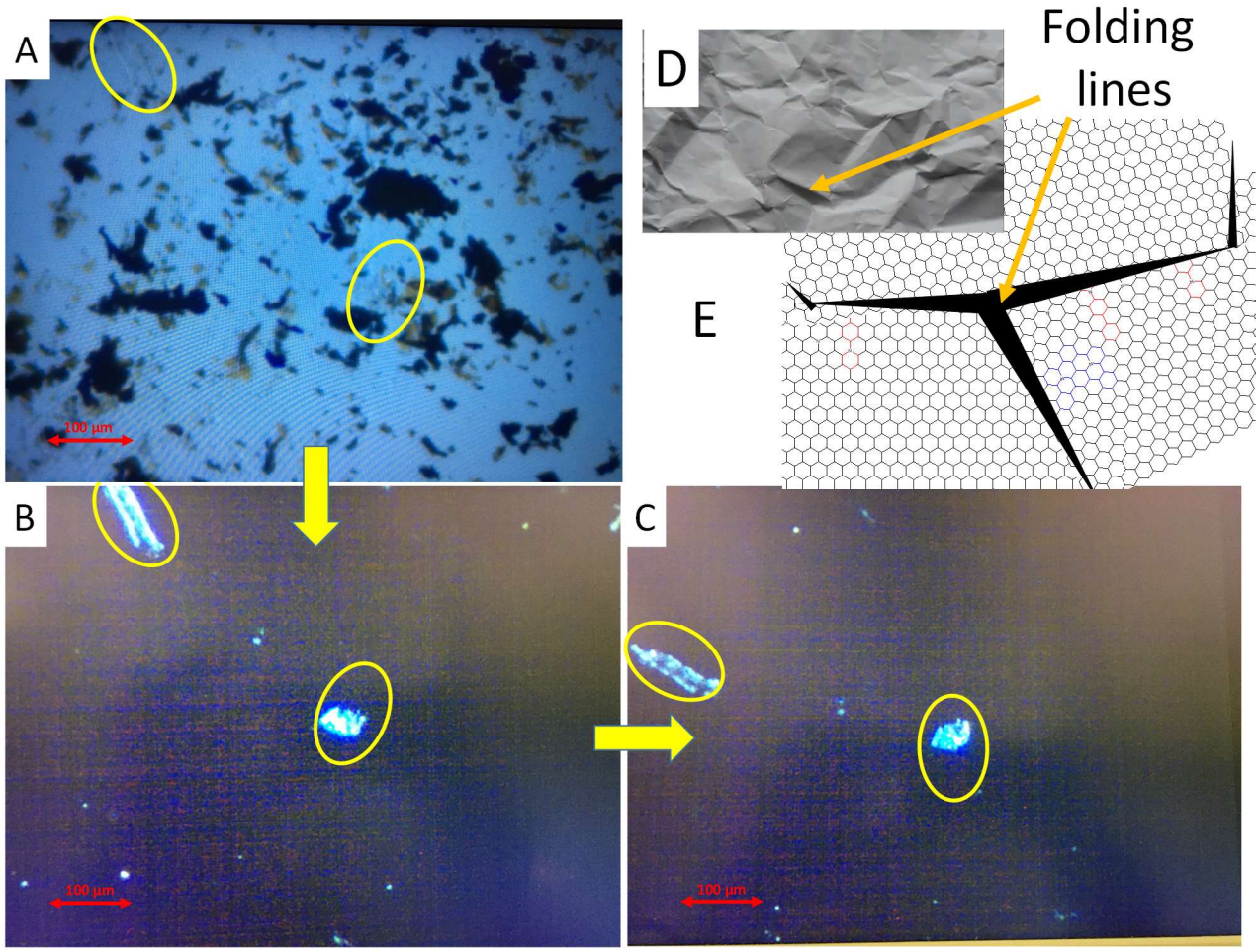

Figure 13: polarised light study of thin C_2N flakes (yellow circles). A): normal light; B): same flakes under cross polarized light and C) same sample upon rotation. The appearence of the flakes alternatively goes brighter and darker as a function of the angle. D) and E): a simple model accounting for the observation of different domains inside a single flake.

XRD.

A compared XRD analysis of a crude and washed C_2N sample was performed. The results are shown on Figure 14.

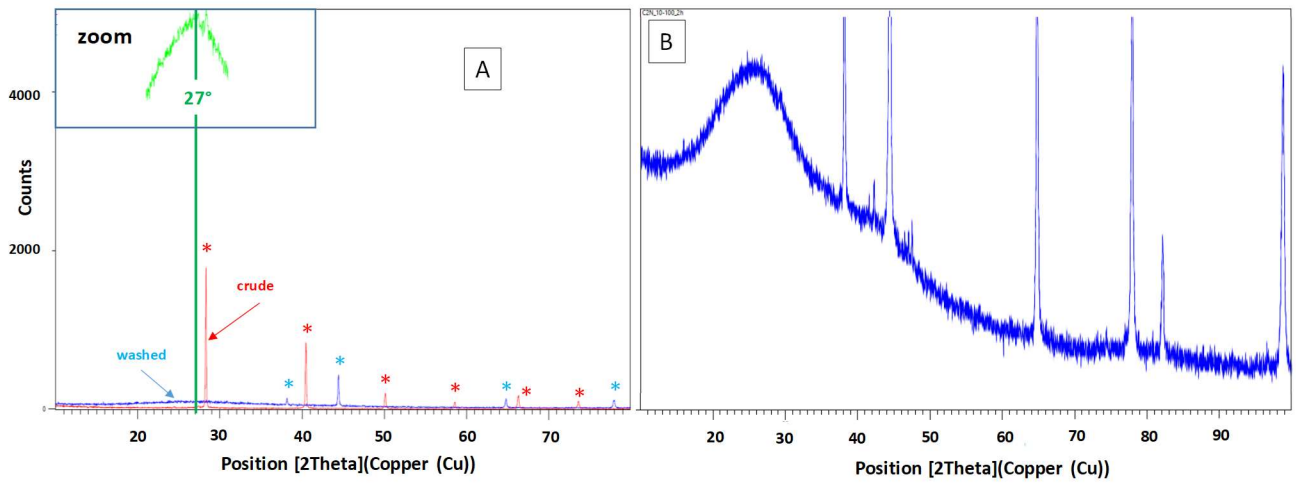

Figure 14: A) compared powder X-ray diffractograms of a crude (red) and washed (blue) C_2N samples (same batch). Insert (green): zoom over the blue curve. Blue stars : signals from the aluminum sample holder ; red stars : signals from KCl by-product. B) : Powder x-ray diffractogram of the washed C_2N sample. Black stars : signals from the aluminum sample holder.

The same trends as the ones observed with CN are evidenced. The crude sample (Figure 14A, red) only shows signals from the KCl by-product. However, the same sample shows a broad peak, centered at 27° (Figure 14A, insert) after washings (Figure 14A, blue). This signal was absent from the crude sample. Once again, it can thus be concluded that i) the flakes mostly exist as individual/few layers objects in the crude material, getting aggregated during washings, and ii) they are thus likely to grow individually during the synthesis.

Figure 14B shows the powder X-ray analysis of the washed sample. The presence of the peak around 2θ=27° shows that the material has a layered structure. The broadness of the peak evidences an irregular spacing between the sheets. Indeed, as the sheets get agregated during washing, some foldings and/or inclusion of residual solvents occurs between the layers, resulting in a broad distribution of interplane spacings. A shoulder around 2θ=40 degrees corresponds to the in-plane signal [46, 52].

XPS

The compositon of washed samples was assessed by XPS analysis (Figure 15). A survey shows the presence of the expected elements, C and N. A prominent peak of oxygen is also observed. It may be due to the presence of trapped oxygen-containing species, a commonly observed feature with this type of material [43, 46, 51, 52].

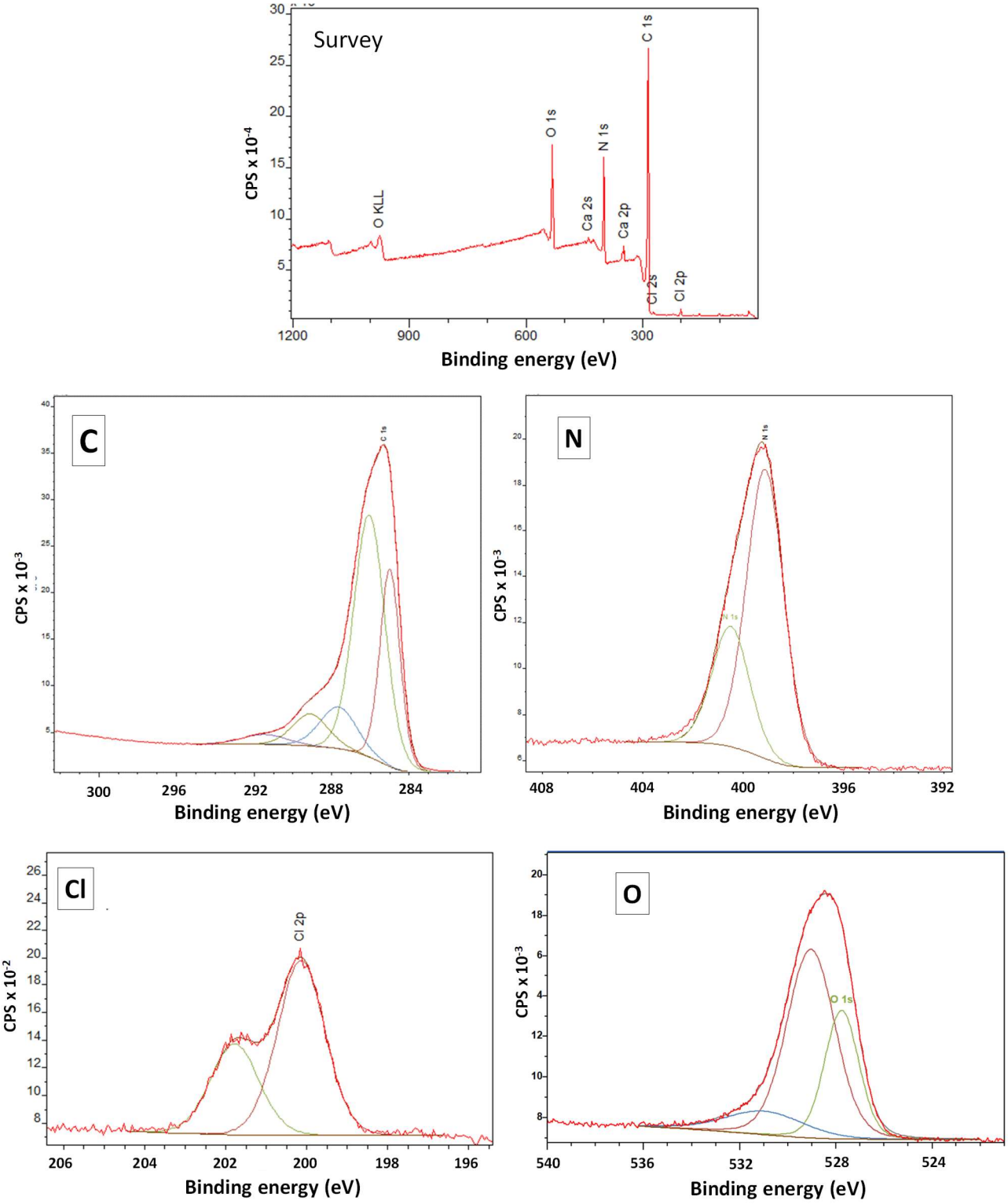

Figure 15 : XPS analysis of a washed C_2N sample.

The deconvolution of the C 1s peak shows two main components, at 285,9 eV (C=N) and 284.9 eV (C-C). This later peak, ubiquitous, may originate from contamination. The former one is associated with the C=N bonds of the 2D framework. Minor peaks at higher binding energies are from C=O containing adsorbed contamination, commonly encountered in XPS analyses. These may also orginate from the interaction between N and included species (protons, as the material was washed with HCl, or remaining metallic cations), in line with the observed features of the N 1s signals. Indeed, the

corresponding electron-withdrawing influence may affect as well the adjacent N-bonded carbon atoms (see below).

Regarding the N 1s signal, it may be deconvoluted in two components, at 399.12 and 400.46 eV. The first one is attributed to pyridinic-type N, commonly observed between 398 and 399 eV, as discussed in the previous paragraph. [38, 39, 40, 41]. Ideed, our synthesis does not involve any kind of NH_2 -type species (that appear in the same binding energy range), thus ruling out this possible attribution. Moreover, the dark black appearence of our material excludes any kind of reduction reaction (that could result in the formation of N-H species), that would break the conjugation of the network, rendering the material colorless. Moreover, tetrachloropyrazine was introduced in close to stoechiometric amount vs. potassium. It thus excludes a possible overreduction of the C_2N backbone to N-H containing species, as this would need significant amounts of excess metal. Moreover, as the post-synthesis workup was done under ambient conditions, such adventitious reduced species would have been re-oxidized to the main C=N ones (especially under the acidic conditions used for the redispersion of the material).

The High energy component (400 eV) may be attributed at first sight to residual tetrachloropyrazine. However, this later interpretation is ruled out, as the amount of remaining C-Cl in the product is very low (Figure 15, survey). The first interpretation also seems unlikely, as these by-products are recovered in the supernatant and the corresponding amount of materials is very low.

This high energy component is better attributed to the interaction of pyridinic nitrogens with included, remaining metallic cations or hydrogen-bonded impurities that appeared during post-synthesis workup. Indeed, it was shown that the exact value of the position of the N 1s peak is strongly dependant on the environment of the corresponding nitrogens [38, 39, 40, 41]. This last interpretation is in line with the presence of oxygenated species (Figure 15, O1s analysis) and remaining potassium and calcium. The C/N ratio is 3, higher than the expected value of 2. This may be ascribed to commonly observed carbon contamination of the sample. As said before, traces of chlorine are also observed (Figure 15), with binding energies associated with C-bonded chlorine. This confirms the very small amount of defaults lefts in the flakes, as only a very small amount of unreacted pyrazinic C-Cl bonds are present in the material.

SEM/EDS

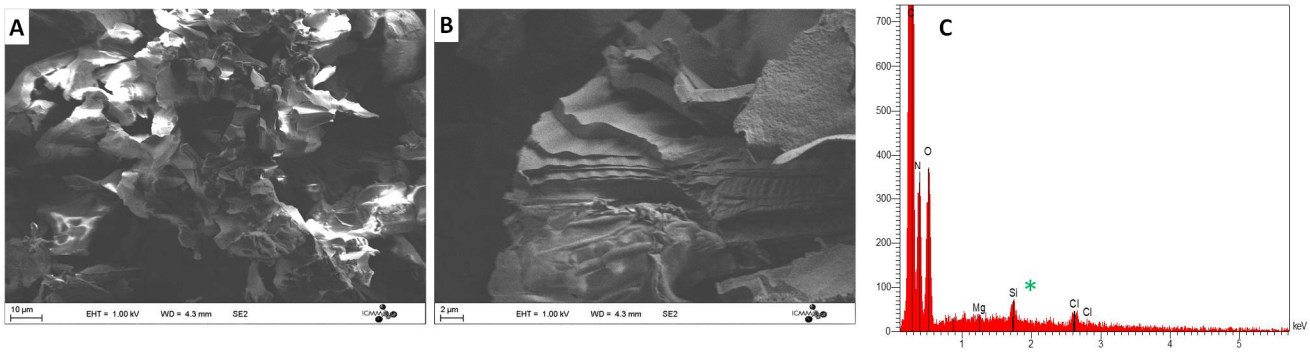

Figure 16: SEM imaging (A and B) and EDS analysis (C) of a C_2N sample (after washings). Green star: artifact from the substrate

SEM observation of an as-prepared sample (Figure 16) shows the presence of large flakes (>10µm). Their layered structure after washing and drying is in accordance with the expected one for C_2N [43]. EDS (figure 16C) shows the presence of the expected elements, along with SiO_2 from the surbstrate.

TEM.

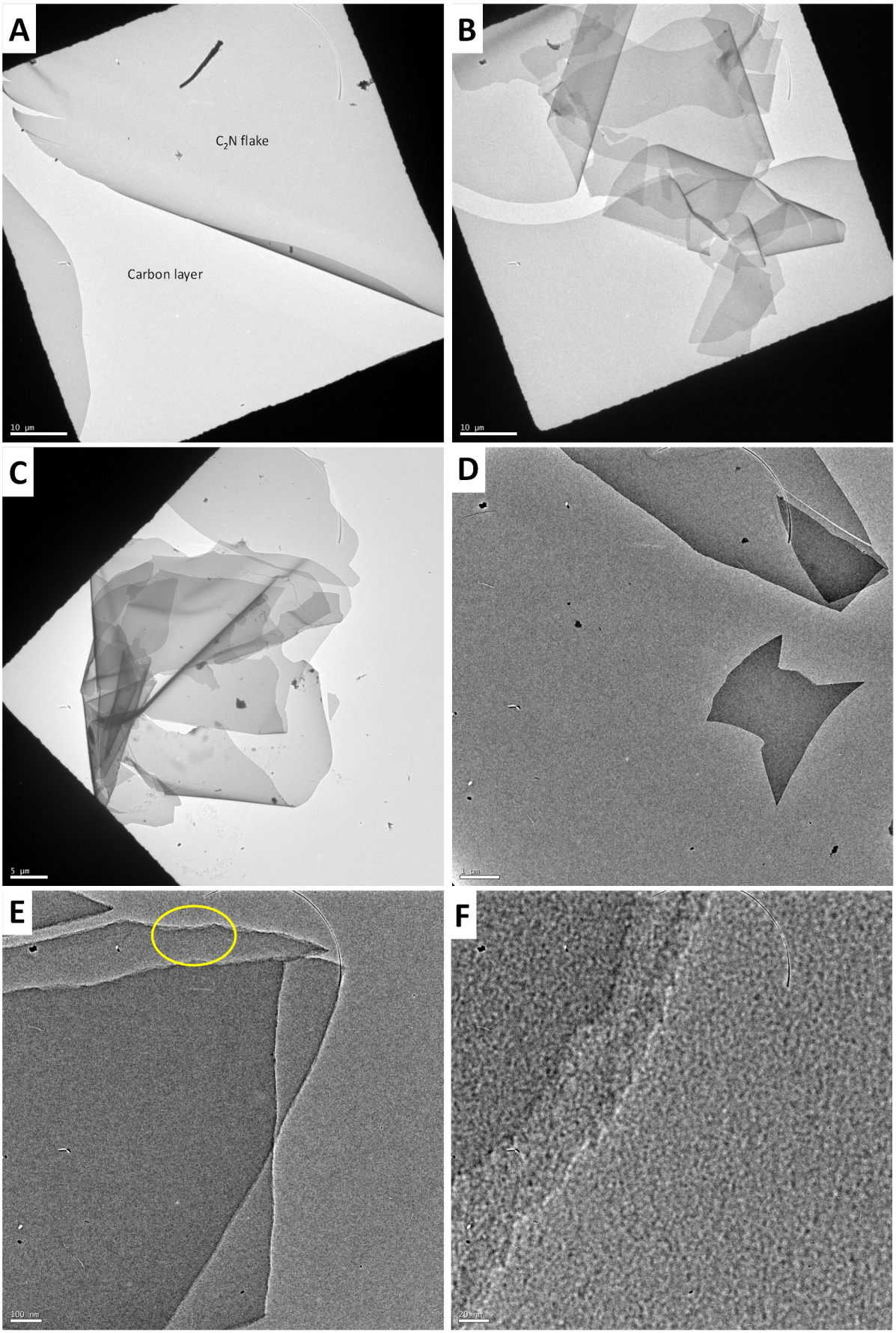

Figure 17 : A→F: TEM analysis of a C_2N sample at increasing magnifications.

Extensive TEM analyses were performed with washed samples. Different solvents were tested to optimise the dispersions (see supporting informations, Figure S2G). Figure 17A shows a typical image of a C_2N sample, washed according to the following sequence : 1) acetone, 2) water ; 3) HCl (see S2). HCl was shown to be the best choice for the redispersion of the different materials, in accordance with previous observations [55]. The images on Figure 17 are shown at increasingly high magnifications, to assess the quality of the flakes over different scales. Very large and smooth flakes are observed, with sizes exceeding 100 µm (Figures 17A and B, others micrographs of HCl-dispersed samples are provided in S2G-c). Some flakes are so large that they were first misinterpreted as broken carbon films from the TEM grid. However, a detailed analysis of the micrographs showed that: i) some typical features of carbon grids next to the flakes are still observed, and ii) the contrasts next to different flakes on different squares were found similar, thus proving that the carbon film was still present. The flakes are rather thin, beeing quite transparent to the e-beam. A detailed observation of the edges of these flakes shows that they're made of few layers. (Figures 17E and F yellow circle).These flakes appear as defects-free over very large areas (even at high magnifications, (Figures 17D→F)), assessing their structural quality. In some cases, these flakes were found to roll, forming tubular structures reminiscent of carbon nanotubes (Figure S2H).

The obtained C_2N material thus exhibits similar characteristics compared with the ones of the previously described CN.

A detailed observation of the edges of the flakes (Figure 18A, yellow circle) shows a regular pattern (Figure 18B, zoom Figure 18C), exhibiting a characteristic distance around 0.5 nm (Figure 18C). Note that this pattern is observed all the edge of the flake long (Figure 18B).

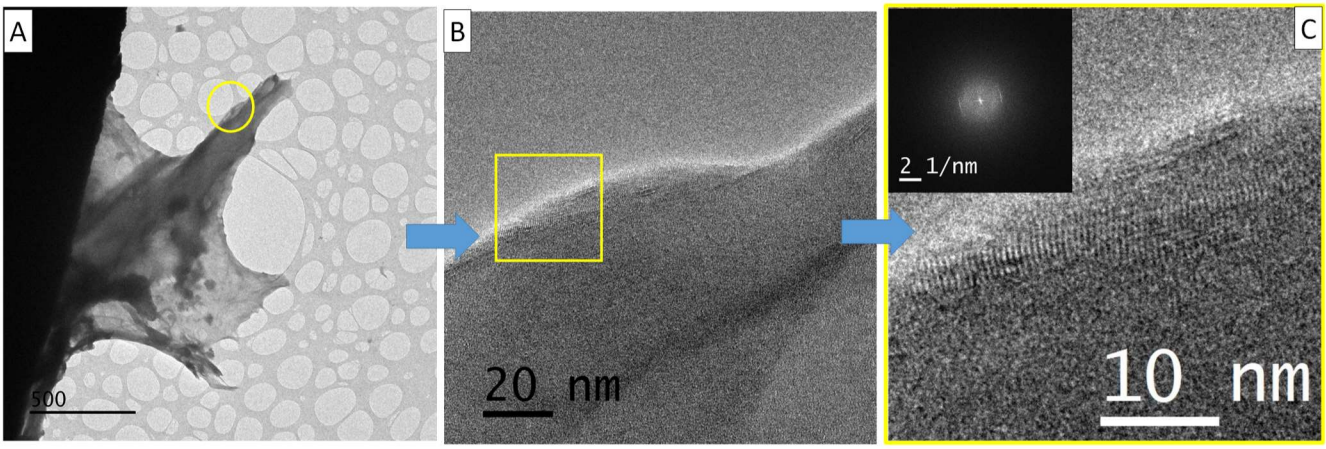

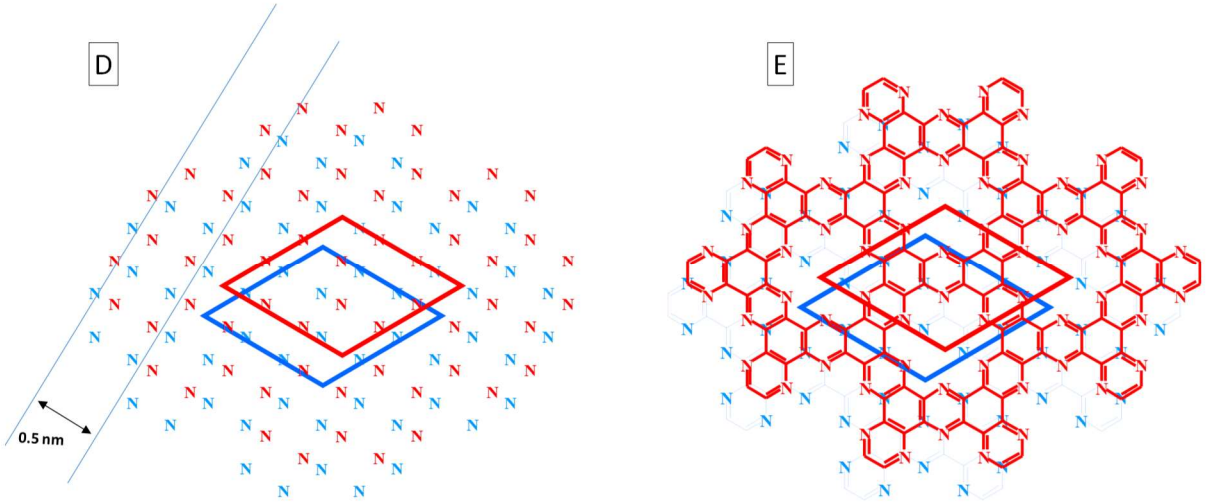

Figure 18 : TEM analysis of a C_2N flake showing a moiré effect. A) the observed flake; B) zoom over the yellow circle figure A; C) zoom over the yellow square Figure B) (insert: FFT of the image); D) two stacked C_2N layers (blue and red,only nitrogen atoms shown for clarity, unit cells of the two stacked layers shown as rhombus) exhibiting the observed 0.5 nm distance.

This pattern is attributed to a moire effect between few superimposed layers. One possibility is exemplified on Figure 18D, with two superimposed layers with an AB type stacking. This moire effect evidences the crystallinity of the whole flake, as there's no reason for it to be more crystalline at its edges. Note that the material degraded very rapidly under the influence of the e-beam. Such an instability of 2D materials under TEM analyses is well documented in literature [56]. Figure 18E details the observed stacking mode. Note that it appears quite similar to the one expected from simulations [57].

We were not able to get convincing electron diffractions patterns from this material. This may be due to the previously mentioned instablity of the material under electron irradiation. In some instances, clear diffraction patterns were observed (one example Figure S2N). However, these were finally considered as artifacts as i) the characteristic distance associated with the [100] plane was not observed, and ii) the brightness of the spots was too high to be associated with few layers flake. These artifacts may be due to remaining inorganics trapped inside the material. Great care should thus be taken while analysing the SAED of layered 2D materials.

EELS

An EELS analysis of a C_2N thin flake is shown on Figure 19. The presence of nitrogen is only observed on the flake (Figure 19B), not on the carbon grid (Figure 19A). C_2N appears as oxygen-free (Figure 19C). This confirms that the oxygen signals observed by XPS analysis are probably due to contamination, or to adventitious oxygen-containing species trapped between aggregated flakes. The near edge structures observed for the C and N signals confirms that these elements are sp^2 hybridized in the material [58].

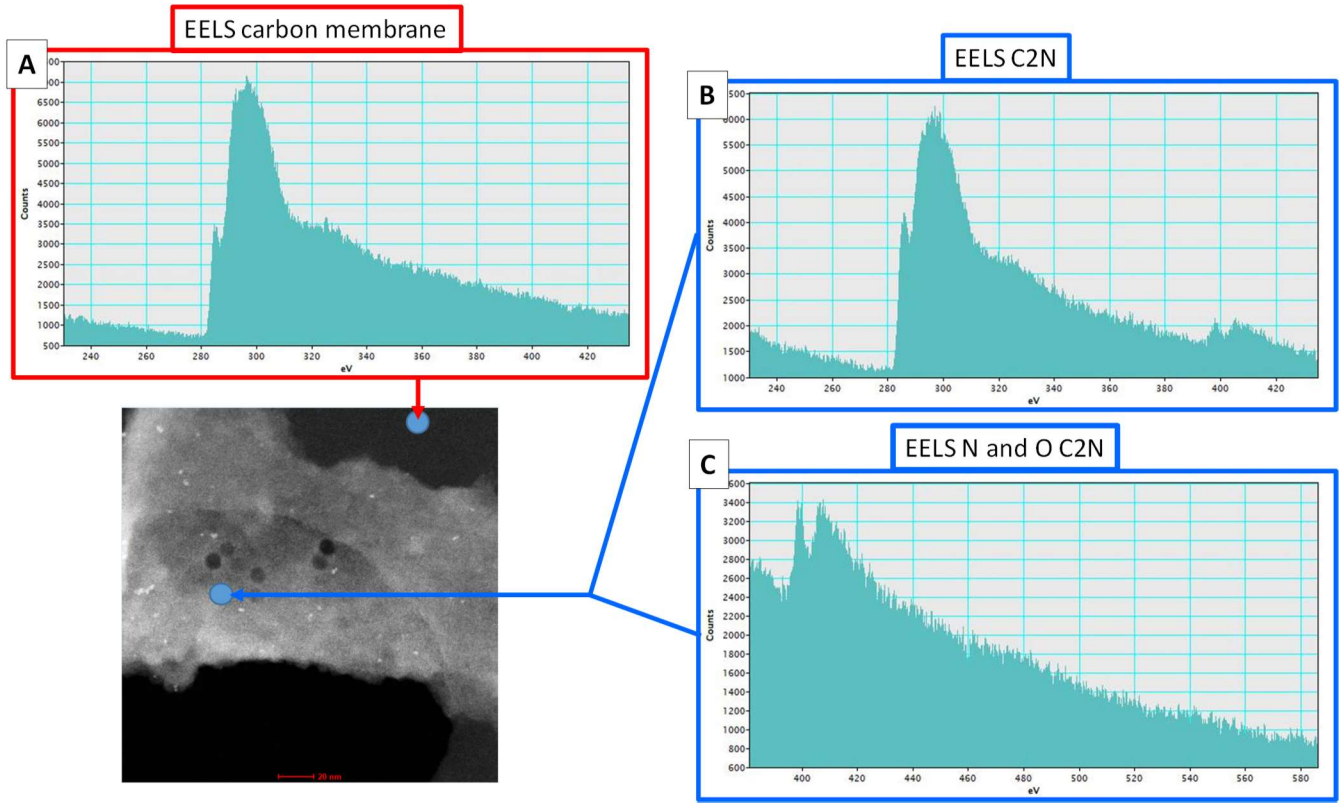

Figure 19 EELS analysis of a single C_2N flake suspended on holey carbon grid. A): carbon grid analysis, B) and C): C_2N sample. The regular, circular holes observed on the sample are due to electron-beam-induced damages.

C) : synthesis of a triazine-based COF

The potassium-promoted reduction of polyhalogenated aromatic building blocks thus appears as a very efficient tool for 2D materials synthesis. We then decided to further expand the scope of this process threw a third example, sketched on Figure 20. This material belongs to the so-called Covalent Triazine Frameworks (CTF) family. These materials are indeed receiving an ever increasing interest, due to their interesting properties for example in the field of photocatalysis [59 60 61].

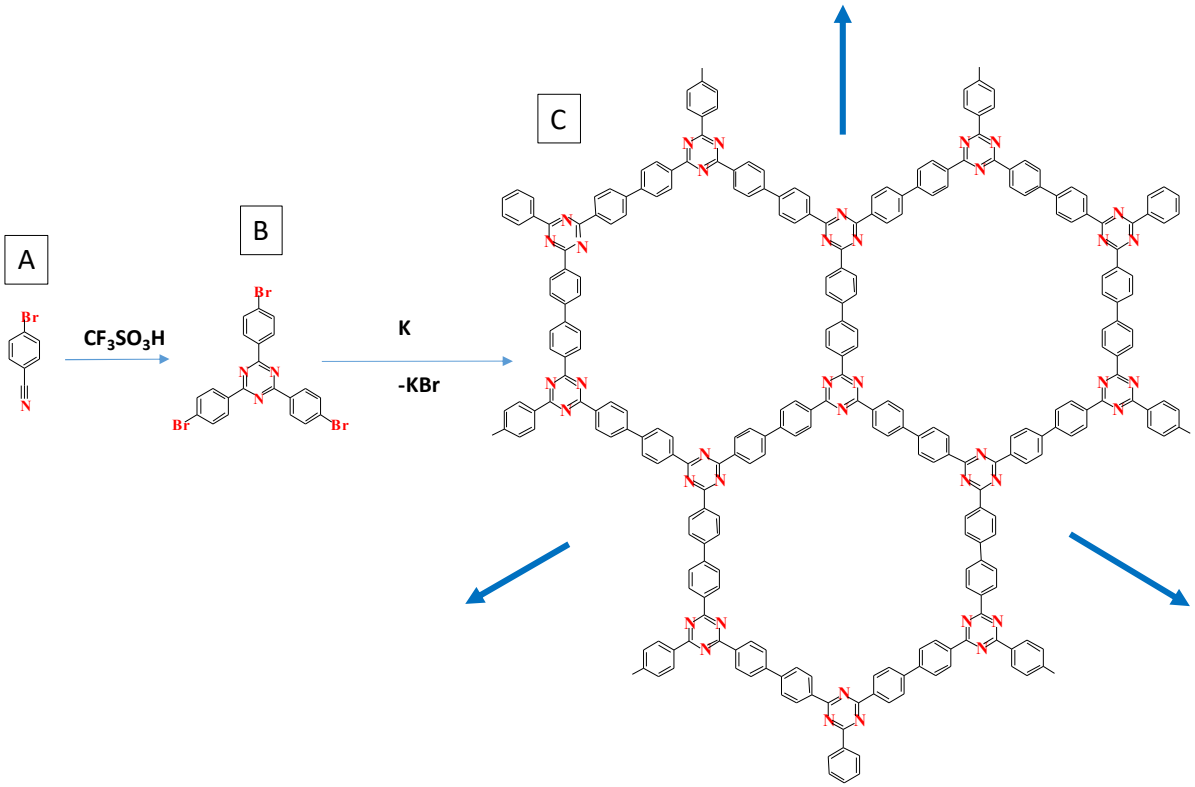

Figure 20: Synthesis of 2D material by reduction of a polyhalogenated triazine derivative.

The starting tris(bromophenyl) triazine **B** was synthesised by acid-promoted trimerisation of 4-(bromo)benzonitrile **A** [62]. The synthesis/purification of CTF-2D material is detailed in the Supporting Informations (S3).

Interestingly, a detailed obervation of the surface of the solid material during the reaction (S3A→E) shows that it grows in a bark-tree like fashion (S3F, orange circle), along with KBr scales (S3F, yellow circles), both visibles with the naked eye. This concomittant formation of layered KBr / CTF (see below) strongly supports our initial assumption that the inorganic by-product (KBr in this case) is likely to favor the confined growth of 2D materials.

Optical microscopy

The CTF material is obtained as a green-brown powder after drying, washing with dichloromethane and water (Figure 21A).

An observation of this material (as a water suspension) by optical microscopy shows it to be made of very large, thin flakes, with sizes ranging from a few µm to 500 µm (Figure 21B). More images are provided in the Supporting Informations (S3G→i). The characteristic features of 2D materials (such as foldings) are easily observed (Figure 21C, center image). The flakes appears as nearly transparent, evidencing their small thickness and large bandgap. Their yellow-green color is quite similar to the one observed using a different synthesis of this material [59]. Needle-like crystals of the starting material are sometimes observed (Figure 21C, yellow circle), as this starting tris(bromophenyl)triazine is highly insoluble and difficult to remove completely.

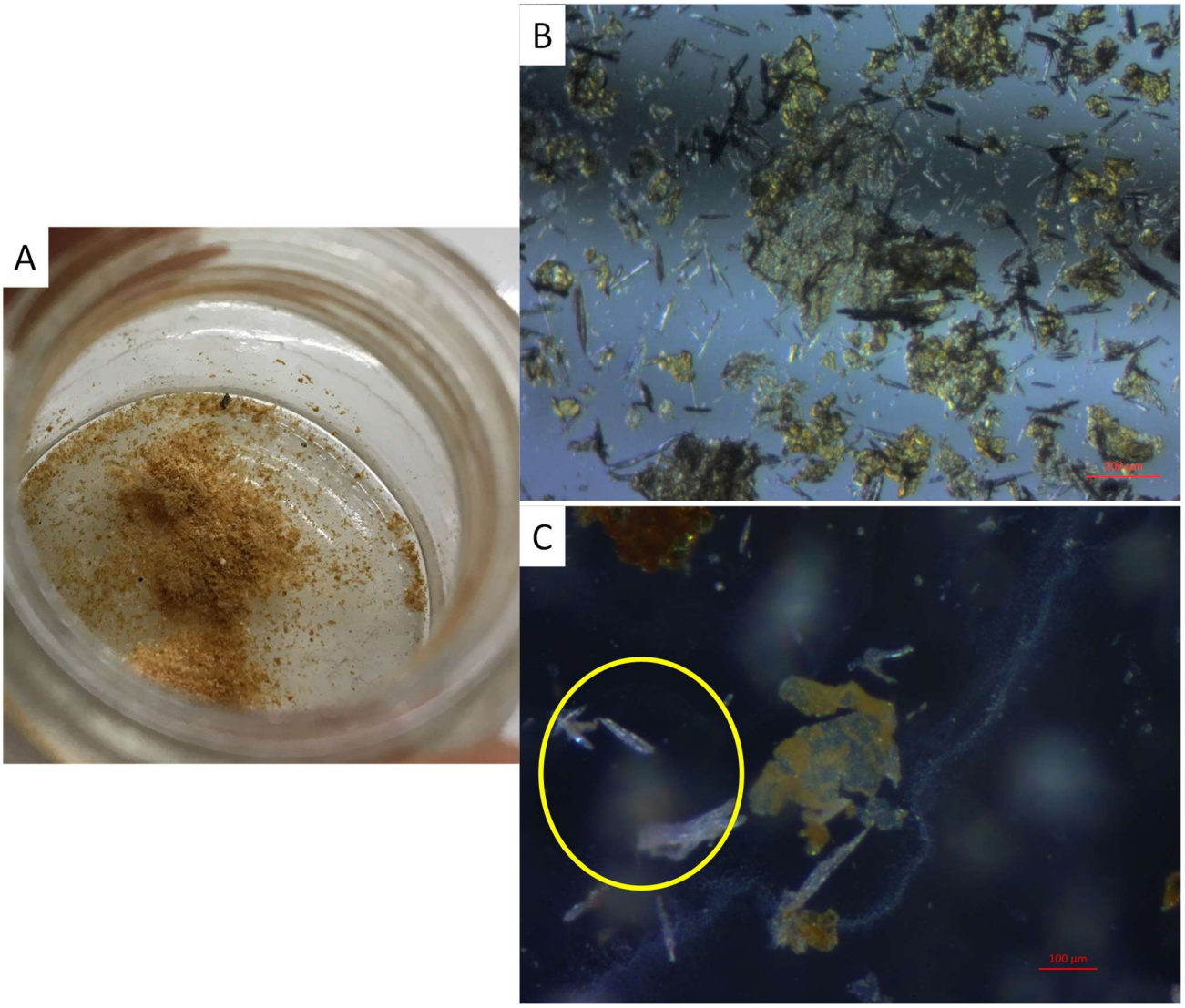

Figure 21: A) crude CTF 2D material ; B) and C) optical microscopy of CTF 2D material, yellow: starting product.

As for the previously described materials, we also found that some flakes (thin enough and not too crumpled), suspended in dispersion oil do rotate the polarisation plane of incident polarised light, as expected for single crystals. One example is shown on Figure 22. Another example is shown on S3M. These extremely thin flakes are nearly invisible (even with the microscope). They can only be detected due to their changing brightness under polarized light.

Note that the observation of other 2D materials such as single layer graphene using polarised light has already been reported [53, 54].

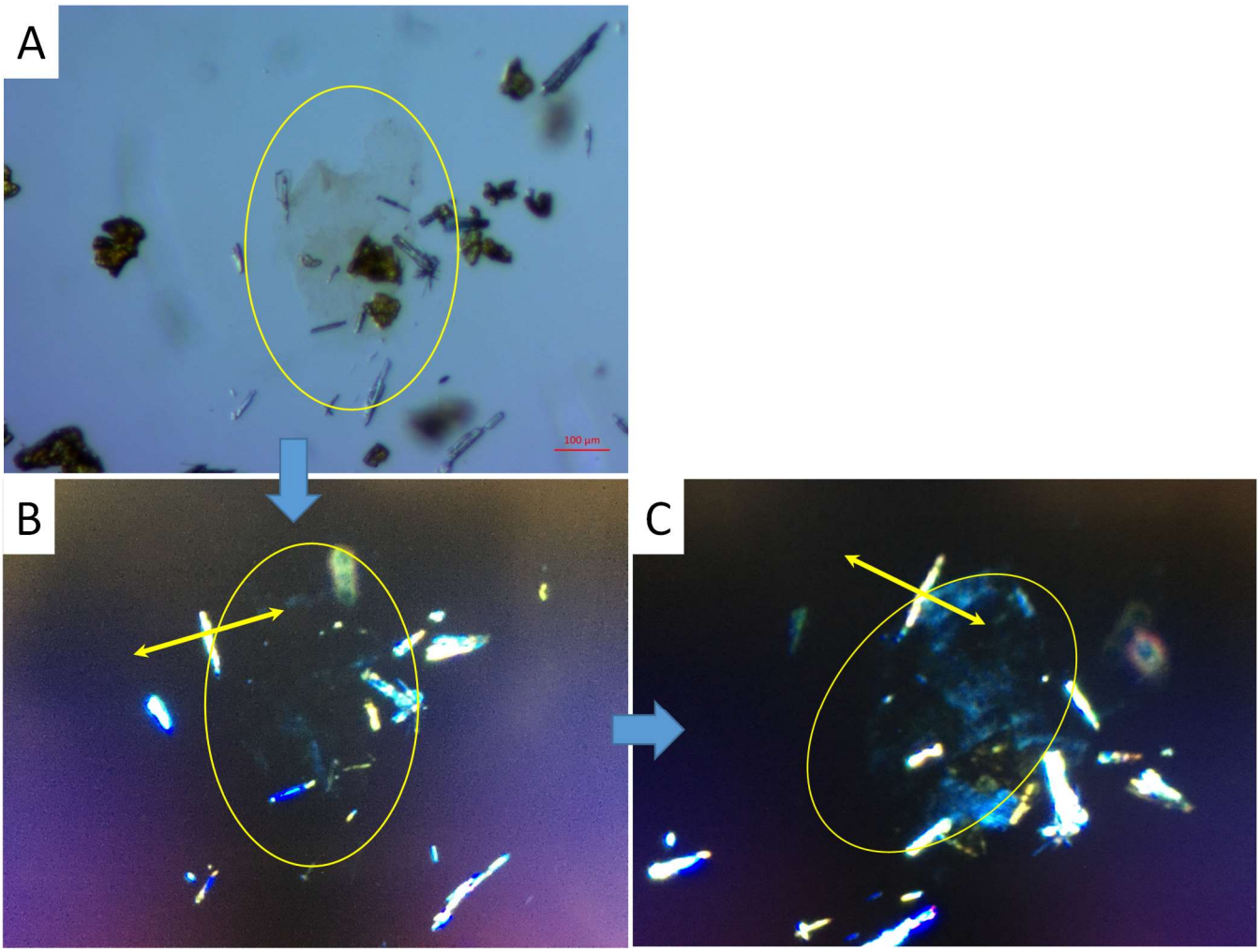

Figure 22: polarised light study of a thin CTF 2D flake (yellow circle). A): normal light; B): the same flake under cross polarized light and C) same sample upon rotation (yellow arrows on B and C as a guide to the eye). The appearence of the flake alternatively goes brighter and darker as a function of the angle. Bright crystals of the starting product are also observed.

SEM

Figure 23 shows an SEM image of CTF-2D material. The presence of large, folded flakes is clearly evidenced. An EDS analysis of such a flake shows the presence of C, N and oxygen-containing contamination (Figure 23). Note that the N signal is absent from the carbon substrate used for this experiment (Figure 23A). The low relative intensity of the N signal is ascribed to i) the low intrinsic relative amount of carbon in the material ($C/N_{theo}=7$), and ii) the presence of the underlying carbon substrate.

In the same way, an EDS analysis of the needle-shaped objects sometimes observed with the CTF flakes shows the presence of bromine along with C, N and O. This confirms the attribution of these needle-shaped objects to the starting product (S3i). A comparison between the EDS analyses of CTF-2D material and the starting product shows that the relative C/N ration is close in both cases, as expected.

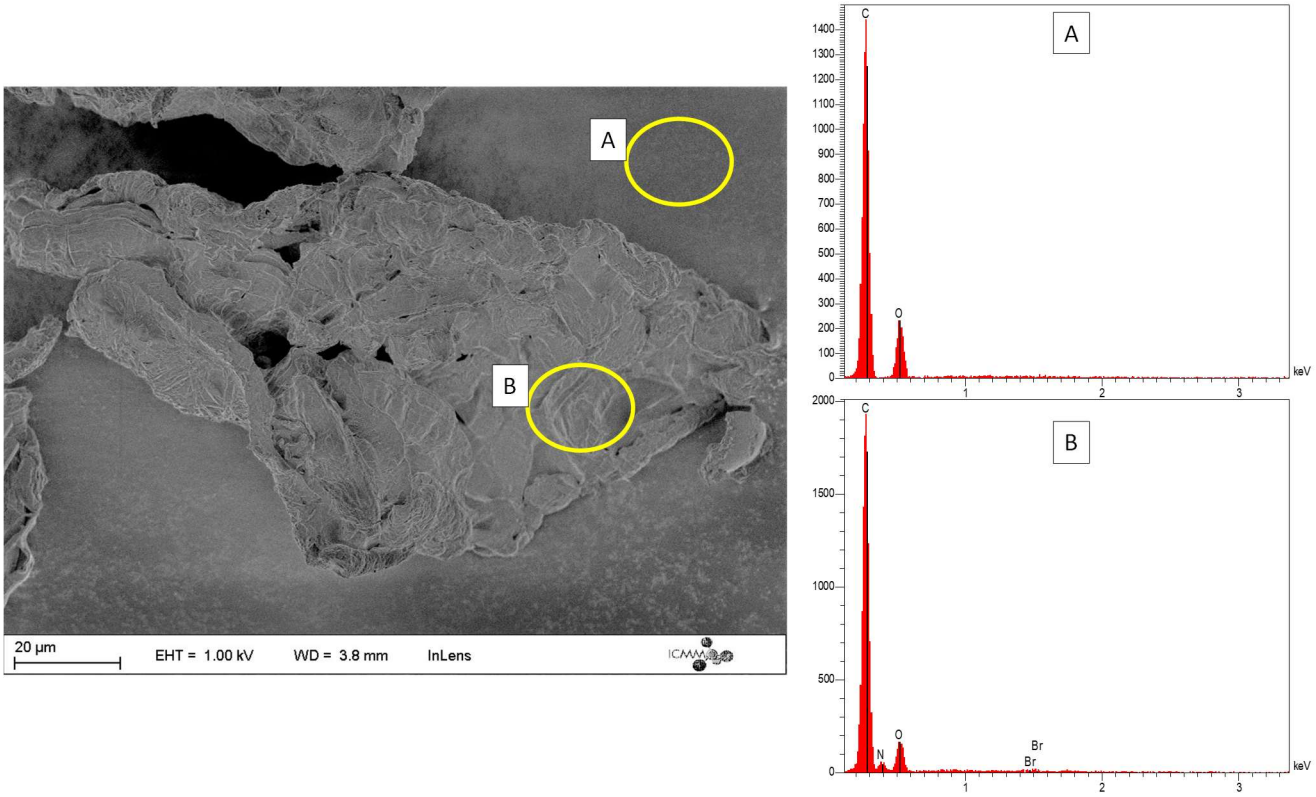

Figure 23: SEMM/EDS analysis of CTF-2D material. A) carbon substrate, B) CTF.

TEM

Figure 24 shows a TEM analysis of the CTF 2D material. As for the two previous materials, the images are shown at increasingly high magnifications, to assess the quality of the flakes over different scales. It confirms CTF material to be made of very thin and large flakes, with length sometimes exceeding 100 µm (Figures 24A and B). The flakes appear as very homogeneous and seemingly defect-free, even at large magnifications (Figures 24C and D). In a few places, some contamination by what seems to be needle-shaped crystals of the starting product are however observed (Figures 24E and F), in accordance with optical (Figure 21C) and EDS (S3i) observations.

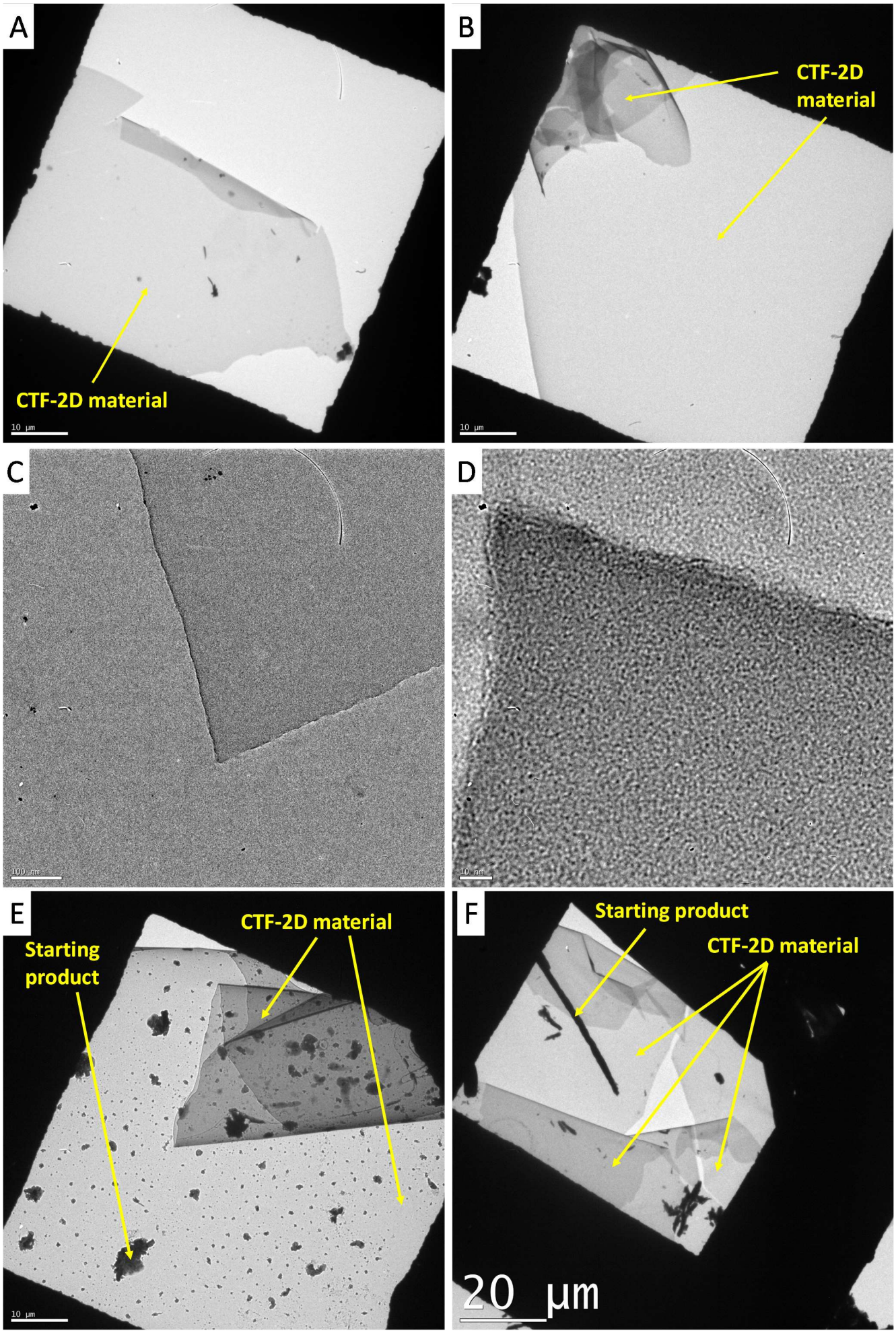
A
CTF-2D material
10 µm
B
CTF-2D material
10 µm
C
100 nm
D
10 nm
E
Starting product
CTF-2D material
10 µm
F
Starting product
CTF-2D material
20 µm

Figure 24: A→F: TEM analysis of CTF-2D material at increasing magnifications.

Some rare, highly folded CTF flakes were sometimes observed. A careful examination of the corresponding high resolution TEM micrograph (one example Figure S3j) over foldings allows to get a rough estimate of the thickness of the flakes. The obtained values fall between 1.5 and 3 nm, corresponding to 5 to 10 2D layers.

Some rare tube-shaped object were also observed (Figure S3k), reminiscent of a bamboo-like growth of carbon nantotubes [63]. This may be due to a molding of potassium droplets during the growth

Figure 25B shows the SAED pattern obtained from the flake shown on Figure 25A. This pattern shows the characteristic distance of 2.2 nm expected for the [100] plane of TPTZ. In the same way, a distance of 6 angströms along the z axis is observed (corresponding to the thickness of two conjugated layers) indicative of an AB type stacking.

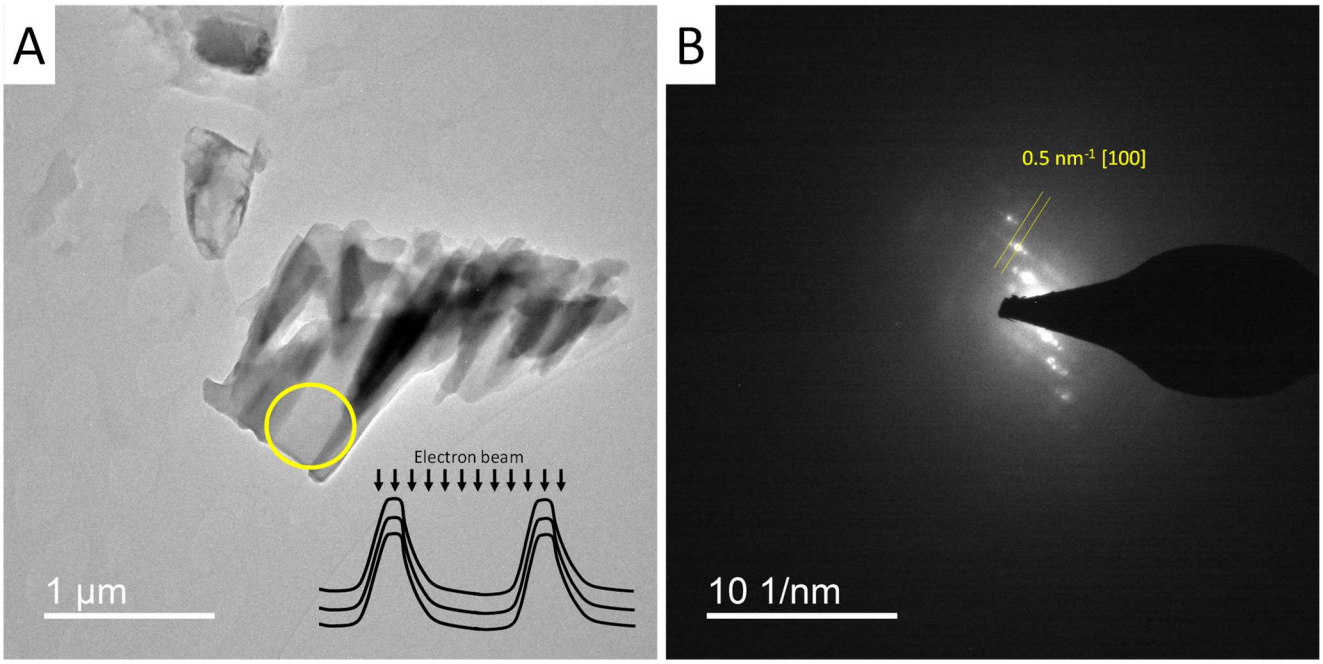

Figure 25: A) TEM analysis of CTF-2D material. Yellow circle: SAED analysed area. Insert: model of the analysed area; B) corresponding SAED analysis.

Such a pattern is observed during SAED analyses of 2D materials where several crystalline, stacked layers are parallel to the incident electron beam (Figure 25A, insert) [64]. It was not possible to observe diffraction on flat-lying sheets, presumably due to their small thickness and the very porous structure of CTF-2D layers. It is likely that in the present case, the observed pattern Figure 25B originates from the folded sides of the studied area (Figure 25A, insert). This experiment confirms that the CTF flakes are crystalline.

Note that (as for the two previous 2D materials) artifacts were commonly observed during SAED experiments (some examples Figure S3l). They were finally discarded after careful analyses, as the charcteristic distances expected for the [100] plane were never observed. These artifacts may originate from trapped inorganic salt, or remaining starting product.

XPS

Figure 26 shows an XPS analysis of CTF-2D material. It shows the presence of strong signals from oxygen and silicon (with a relative O/Si intensity=2), from the silicon wafer used as the substrate for

the analysis. All the expected elements are observed, essentially carbon an nitrogen, with a relative C/N intensity of 12, the expected value beeing 7. This excess carbon is likely to be due to commonly encountered contamination. Only traces of bromine are observed, from remaining, unreacted starting product.

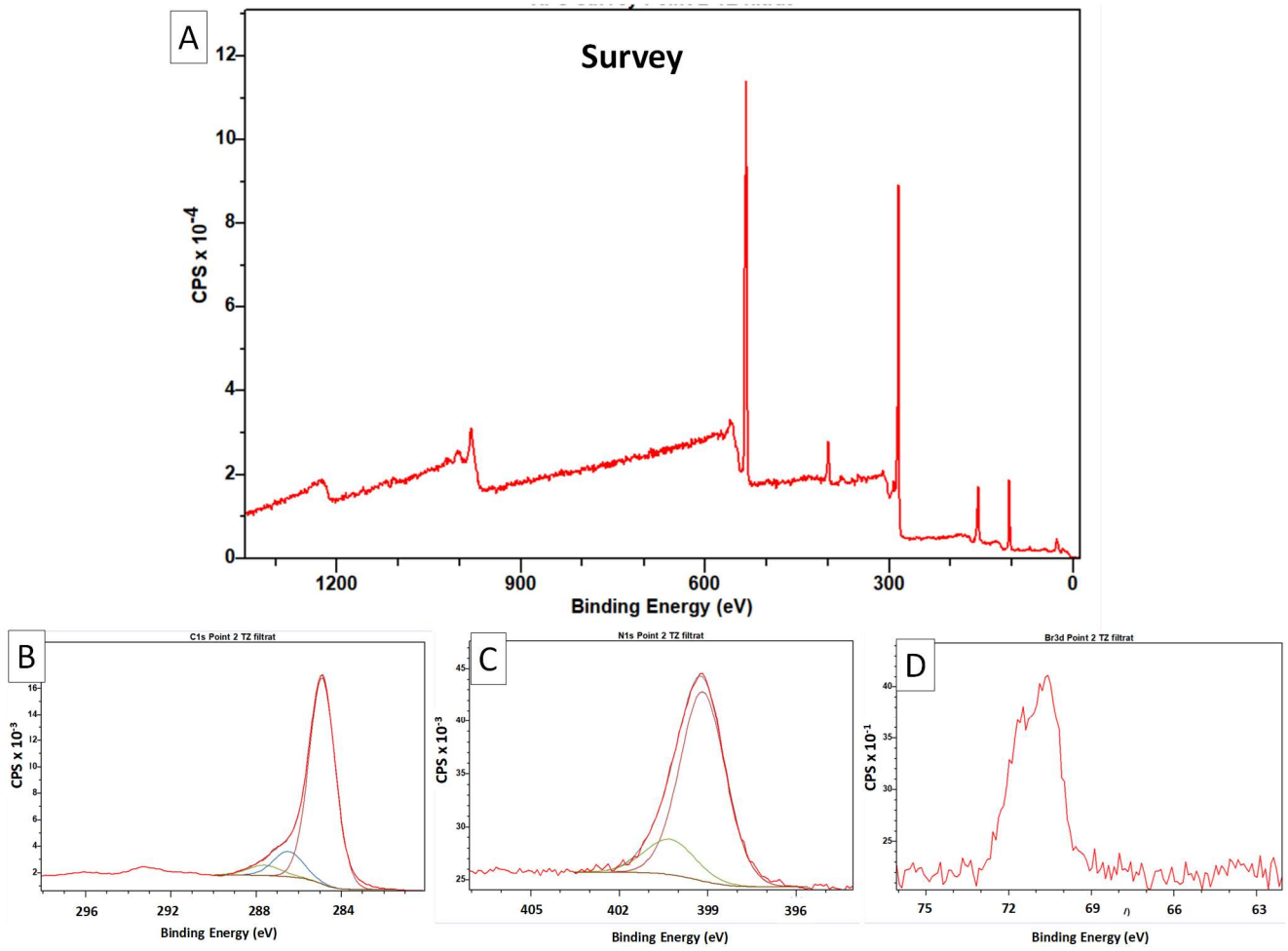

Figure 26: XPS analysis of CTF-2D material. A) : survey ; B) C) and D) C1s, N1s and Br3d respectively

D) Synthesis of C_2N using mercury/potassium amalgam

In line with the « double confinement » strategy, the synthesis of the C_2N carbon nitride (Figure 11) was also realised using another kind of reactive metal interface, the mercury/potassium amalgam. Indeed, the propensity of mercury to form liquid alloys with many metals, including alkaline ones is well know. We reasoned that under these conditions, the metallic interface should be more stable, as mercury itself is not reactive towards tetrachloropyrazine. This could in turn favor the formation of even higher quality 2D layers. Moreover, the liquid nature of the mercury/potassium amalgam should allow for a continuous supply of metallic potassium to the organic solvent/metal interface thus compensating for its consumption during the formation of the C_2N 2D network. Last, the inorganic by-product (KCl) is completely insoluble in the solvent used for the reaction (toluene), thus increasing the confinement effect. The details of the process are to be found in the Supporting Informations (S4A).

The initially shiny mercury interface rapidly gets covered with an orange-greenish deposit (S4A). The amalgam is removed using a pipette, and the supernating solid is washed with ethanol and water. The material is obtained as a light brown/orange powder, with many orange scales easily visible with the naked eye (Figure 27, yellow circles).

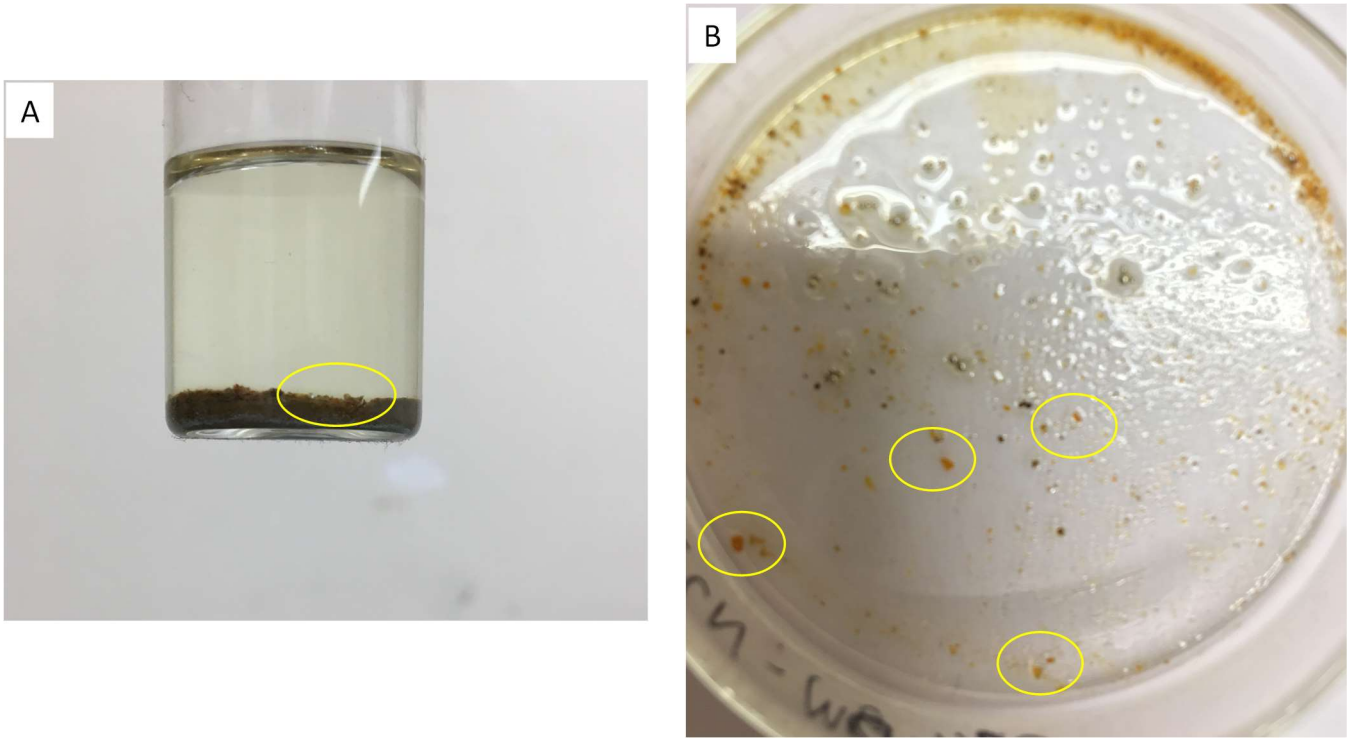

Figure 27: Hg/K-based synthesis of C_2N material. A) crude product, B) after spreading of a droplet of the previous material.

Optical microscopy analysis

Figure 28 shows an optical microscopy analysis of this material (as an EtOH/HCl suspension). Others images are provided in the SI (S4B).

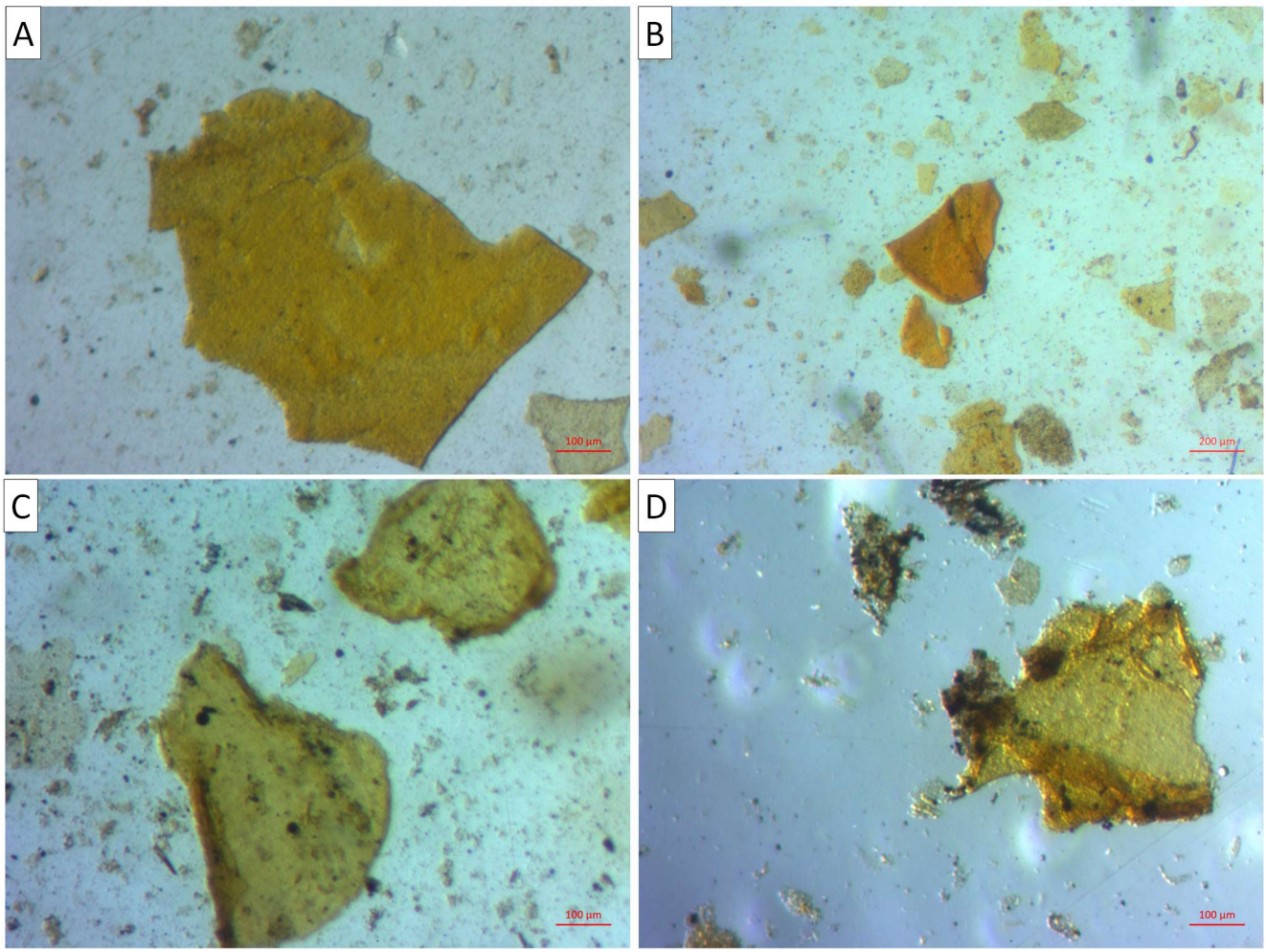

Figure 28: A→D: optical microscopy analysis of C_2N obtained using Hg/K amalgam. The flakes were suspended in a 1 : 2 / EtOH : HCl 2M (v/v) solution.

It shows the presence of very thin (transparent), very large flakes (often mm sized, Figure 28A), all exhibiting the characteristic orange color shades previously observed for thin C_2N flakes. This confirms that the mercury amalgam-based synthesis indeed mostly results in single/few layers flakes. Only a small amount of black materials (strongly agregated/folded flakes) is observed.

A polarised light analysis of these flakes shows them to be quite crystalline, as they alternatively appear bright/dark as a function of the angle between the polarizers (Figure 29). One more example is shown in S4C.

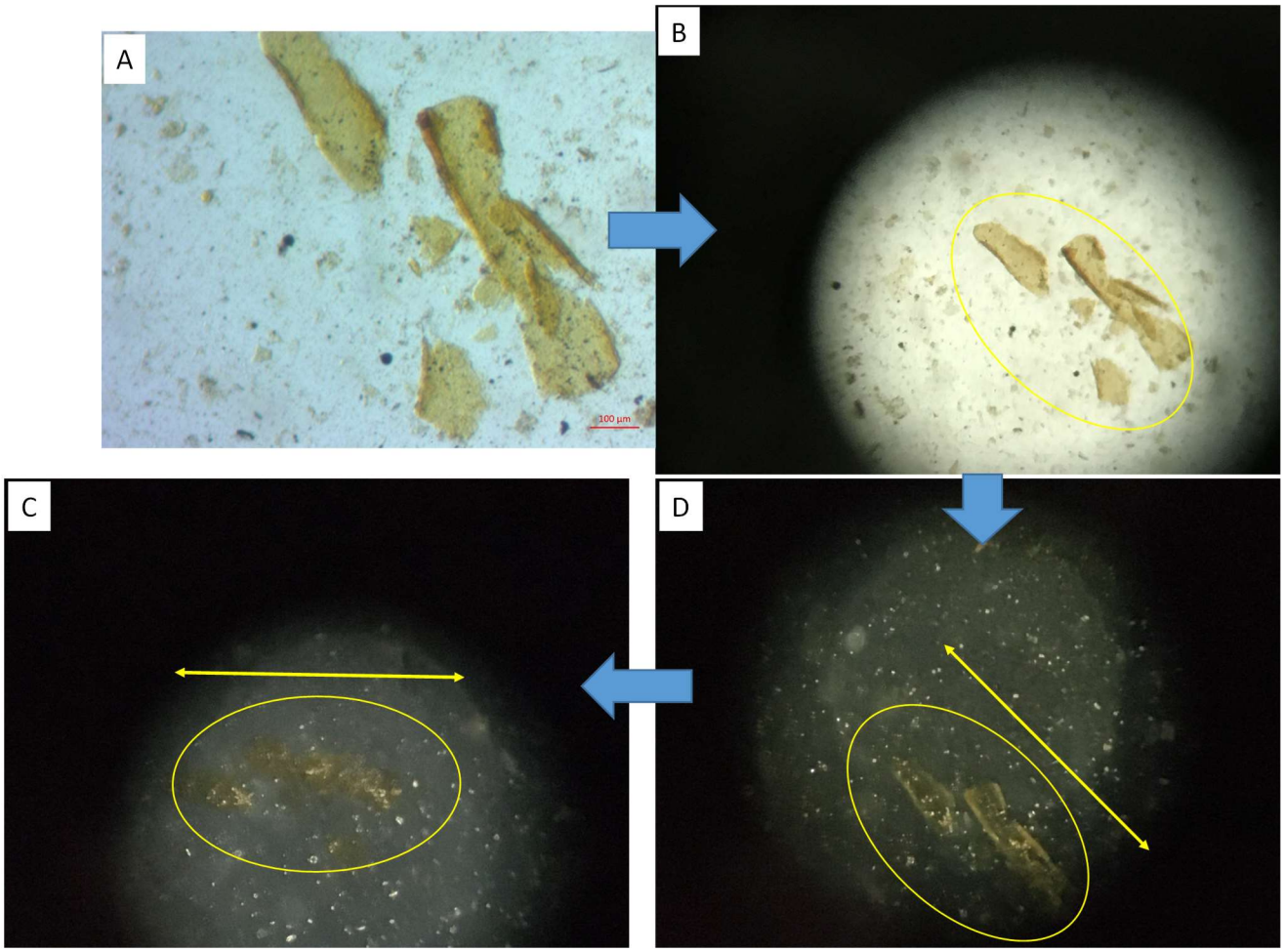

Figure 29: polarised optical microscopy analysis of a broken, tube-shaped C_2N flake. A) and B): normal light. C and D): evolution of the apperance of the flake as a function of the angle between polarizers. The flakes were suspended in a 1 : 2 / EtOH : HCl 2M (v/v) solution.

If kept in suspension for several days, the flakes tend to fold and roll, but are still crystalline (S4D).

TEM

Figure 33 shows a TEM analysis of C_2N obtained using the K/Hg amalgam. As for the previous materials, the best suspensions were obtained in acidic media. In line with the previous C_2N synthesis, very large and smooth flakes are observed, with few visible defects even at high magnifications (Figure 33E→F). An examination of the edges of these flakes clearly shows their layered structure (Figure 33E→F, yellow circles).

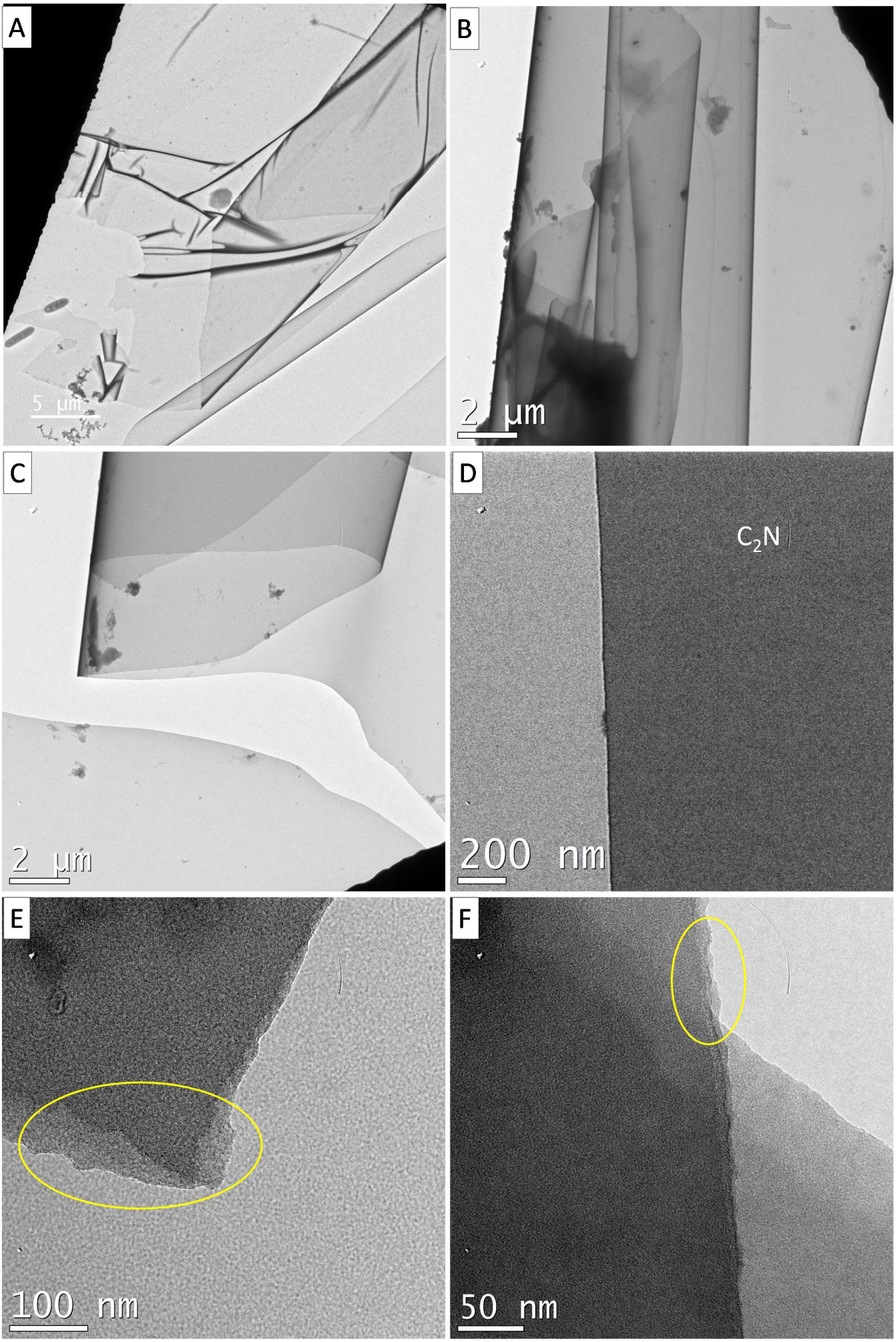
A
5 μm
B
2 μm
C
2 μm
D
C_2N
200 nm
E
100 nm
F
50 nm

Figure 33 A→F: TEM analysis of K/Hg amalgam-promoted C_2N synthesis. The flakes were suspended in a 1 : 2 / EtOH : HCl 2M (v/v) solution.

In order to insure that the observed objects are not artifacts (broken carbon film from the grid), a TEM analysis of the same sample was performed using a holey carbon grid (Figure S4E). It indeed confirms the presence of very large flakes. Some expands over several squares on the TEM grid (Figure S4E-A→E). All are showing the characteristic features of sheet-like materials (folds, overlaps, etc...).

Figure S4F shows a TEM micrograph of a folded, thicker flake, clearly evidencing its layered structure.

Some rare, highly folded C_2N flakes were sometimes observed. A careful examination of the corresponding high resolution TEM micrograph (two examples Figure S4G) over foldings allows to get a rough estimate of the thickness of the flakes. The obtained values fall between 4 and 9 nm, corresponding to 10 to 20 2D layers.

XPS

Figure 34 shows the XPS analysis of one single C_2N flake (Figure 34A) deposited onto a silicon wafer. It first shows the presence of strong signals from oxygen and silicon (Figure 34B) (with an O/Si atomic ratio of 2), from the native SiO_2 layer of the silicon wafer. Carbon and nitrogen are observed (Figures 34C and 34D) as expected. Regarding the N 1s signal, only one single peak is observed, with a binding energy characteristic of pyridinic-type nitrogen atoms [38, 39, 40, 41]. The observed relative C/N intensity is 3, higher that the expected value of 2. This is likely to be due to commonly encountered carbon contamination. This is confirmed by the presence of a strong signal around 285 eV on the C 1s spectra (Figure 34D). Note that this C/N ratio is the same as the one measured for the previously described synthesis of C_2N (using potassium only as a reducing agent). Remainings of mercury (1 atomic %, Figure 34E) and potassium (3 atomic %, Figure 34D) are also observed, due to left starting products/by products. Chlorine is also observed as chloride ions, in a close to 1-to-1 atomic ratio vs. potassium, indicative of the presence of remaining KCl. This confirms the absence of significant amounts of left C-Cl bonds, and thus the formation of a continuous, defaults-free C_2N network. The signal of mercury steadily decreases during vacuuming (Figure 34E), confirming its presence as a metal.

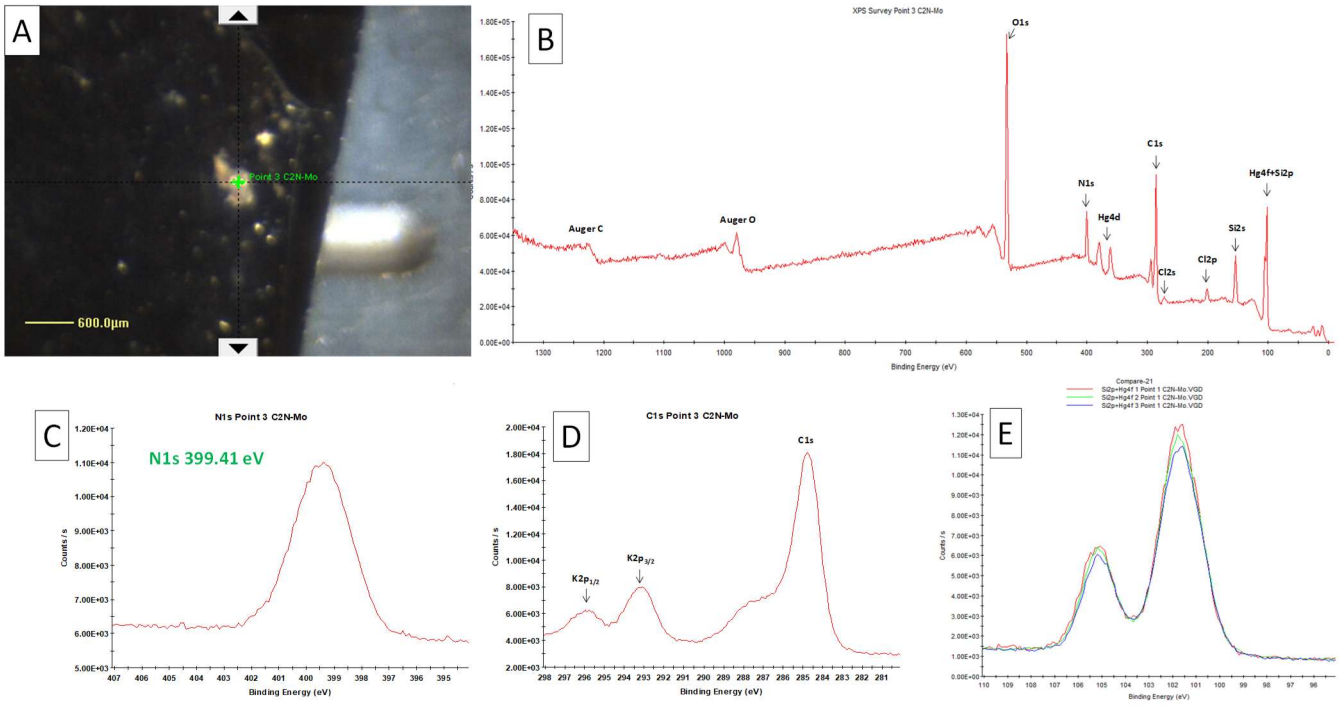

<u>Figure 34</u>: XPS analysis of K/Hg amalgam-promoted C_2N synthesis. A): the analysed flake; B): survey and C)→D): high resolution analyses. The flakes were suspended in a 1 : 2 / EtOH : HCl 2M (v/v) solution. E): evolution of the signal of Hg at the same place as a function of time.

<u>Discussion.</u>

The structure and composition of the 2D materials described in this work are assessed by extensive cross-analyses (optical microscopy/XPS/XRD/SEM/TEM/EDS). Regarding compositions, they are very similar to literature-reported ones, thus assessing the succes of our « double confinment » synthetic strategy. The first example we describe (CN carbon nitride) has already been synthesised using a related protocol (reduction of cyanuric chloride with sodium under high pressure conditions in the presence of nickel as a catalyst [28, 29, 30]. However, the morphology of the material we obtained appears as very different. In our case, very large, well defined and seemingly defect-free 2D layers are obtained. These differences might be related to the difference in reactions conditions, and/or to the smaller ionic radii of Na^+ (Na beeing the reducing agent used in the previously cited studies) vs. K^+. Interestingly, our process lead to a material that easily redisperses in water.

The same features were also observed for the two other COFs described in the present work, i.e. very large, and defect-free flakes with good composition analyses. Accordingly, a comparition between the EDS and XPS analyses of CN, C_2N, and CTF shows a continuous decrease of the relative amount of nitrogen from CN to CTF, in accordance with the corresponding respective theoretical nitrogen contents in their structures.

In the case of CN and C_2N, DRX shows the presence of the characteristic peak associated with interplane spacing [43, 46, 51, 52]. However, this peak exhibits some specific features. First, it only appears after washing the samples. Second it is quite broadened. As TEM demonstrates the very high quality of the flakes, we consider that the broadness of the peak is likely to be due to a broad distribution of interplane spacings. This originates from the fact that the layers grow individually, getting stacked during the washing steps. This may induce an irregular spacing after drying. This may also eases the inclusion of metallic cations inside the coordinating holes. Indeed, a few percents of remaining K and

Ca (a commonly observed impurity in commercial-grade potassium) are present in our CN and C_2N samples.

For the first time, the flakes described in our work are sufficently large and defect-free to behave as single-crystals, as evidenced by polarised light microscopy analyses.

TEM confirms the exceptional quality/crystallinity of the 2D layers of all three COFs. The best dispersions (thinnest and largest flakes) were observed upon treatment of the as prepared materials with HCl, in comparison with the other dispersant that we used. Aqueous HCl is thus the best choice for the suspension/processing of these materials, in line with previous observations [55]. This may be due to partial protonation of embeded nitrogen atoms, inducing electrostatic repulsions between flakes. This may also explain the presence of higher binding energy components in the N 1s XPS analyses.

Interestingly, thin flakes of the three COFs that we synthesised exhibit different intrinsic colors, brown for CN, greenish-brown for CTF, whereas C_2N exhibits a deep orange one. This evidences the smallest bandgap of the later.

It should be underlined here that for all the COFs that we synthesised, the whole materials are made of flakes such as the ones shown on the different figures (both on the paper and in the SI). Indeed, all the observed areas on several TEM grids from different syntheses do show similar objects.

Improving the stability of the metallic interface by using potassium-mercury amalgam considerably improves the quality of the C_2N flakes, as expected for a surface-confined growth process. For the first time, millimeter-scale flakes of C_2N were obtained, an exceptional feature in the field of COFs.

The successful synthesis of three different 2D networks, using very different building blocks shows that our metallic potassium based process appears as quite general. This opens the door towards the synthesis of COFs with more complex structures.

Conclusion.

A simple protocol for the synthesis of graphene-related COFs was designed, and exemplified on three different examples.

The exceptional quality of the resulting materials (in terms of flakes sizes and defect-free nature) shows that the proposed « double confinement strategy » approach appears interesting for the synthesis of high quality 2D materials. This high quality, along with the soft conditions used and common laboratory equiments makes our process a significant improvement in the field.

The fact that the characteristic X-ray diffraction peak around 26° is only observed on washed samples tend to indicate that the growth of these 2D materials occurs as single/few layers, a new feature for wet syntheses of 2D materials.

These materials hold great promises in the field on nanoelectronics (high band gap support for graphene, transport studies, etc…). They're also interesting for photophysics, due to: i) the large size of the crystalline domains, ii) their low defects content and iii) their direct synthesis as highly exfoliated sheets. These studies are underway, and will be reported in due course.

Acknowledgements

We gratefully acknowledge Dr. Frederic Fossard (LEM, ONERA) for some of the elemental analyses shown in the paper.

The present work has benefited from Imagerie-Gif core facility supported by l'Agence Nationale de la Recherche (ANR-11-EQPX-0029/Morphoscope, ANR-10-INBS-04/FranceBioImaging ; ANR-11-IDEX-0003-02/ Saclay Plant Sciences).

Data availability: The datasets used and/or analysed during the current study are available from the corresponding author on reasonable request.

References

[1] K. S. Novoselov et al. Electric field effect in atomically thin carbon films, Science 306, 666 (2004).

[2] Geim, A. K.; Novoselov, K. S. The Rise of Graphene. Nat. Mater. 2007, 6, 183−191.

[3] Radisavljevic, B.; Radenovic, A.; Brivio, J.; Giacometti, V.; Kis, A. Single-layer MoS_2 transistors. Nat. Nanotechnol. 2011, 6, 147−150.

[4] Li, H.; Wu, J.; Yin, Z.; Zhang, H. Preparation and Applications of Mechanically Exfoliated Single-Layer and Multilayer MoS_2 and WSe_2 Nanosheets. Acc. Chem. Res. 2014, 47, 1067−1075.

[5] Vogt, P.; De Padova, P.; Quaresima, C.; Avila, J.; Frantzeskakis, E.; Asensio, M. C.; Resta, A.; Ealet, B.; Le Lay, G. Silicene: Compelling Experimental Evidence for Graphenelike Two-Dimensional Silicon; Phys. Rev. Lett. 2012, 108, 155501.

[6] Oughaddou et al. Silicene: A promising new 2D material, Prog. Surf. Sci. 90, 46 (2015).

[7] Likai Li, Yijun Yu, Guo Jun Ye, Qingqin Ge, Xuedong Ou, Hua Wu, Donglai Feng, Xian Hui hen, Yuanbo Zhang; Black phosphorus field-effect transistors; Nature Nanotechnology volume 9, pages 372–377 (2014).

[8] Balendhran, S.; Walia, S.; Nili, H.; Sriram, S.; Bhaskaran, M. Elemental Analogues of Graphene: Silicene, Germanene, Stanene, and Phosphorene. Small 2015, 11, 640−652.

[9] Liu, H. et al. Phosphorene: an unexplored 2d semiconductor with a high hole mobility. ACS nano 8, 4033–4041 (2014).

[10] Lin, Y.; Williams, T. V.; Connell, J. W. Soluble, Exfoliated Hexagonal Boron Nitride Nanosheets. J. Phys. Chem. Lett. 2010, 1, 277−283.

[11] Song, L.; Ci, L.; Lu, H.; Sorokin, P. B.; Jin, C.; Ni, J.; Kvashnin, A. G.; Kvashnin, D. G.; Lou, J.; Yakobson, B. I.; et al. Large Scale Growth and Characterization of Atomic Hexagonal Boron Nitride Layers. Nano Lett. 2010, 10, 3209−3215.

[12] Zhang, Y.; Tan, Y.-W.; Stormer, H. L.; Kim, P. Experimental Observation of the Quantum Hall Effect and Berry's Phase in Graphene. Nature 2005, 438, 201−204.

[13] Li, X.; Cai, W.; An, J.; Kim, S.; Nah, J.; Yang, D.; Piner, R.; Velamakanni, A.; Jung, I.; Tutuc, E.; et al. Large-Area Synthesis of High-Quality and Uniform Graphene Films on Copper Foils. Science 2009.

[14] Novoselov, K. S.; Mishchenko, A.; Carvalho, A.; Castro Neto, A. H. 2D Materials and Van der Waals Heterostructures. Science 2016, 353, issue 6298, p. 9439.

[15] Radisavljevic, B.; Radenovic, A.; Brivio, J.; Giacometti, V.; Kis, A. Single-layer MoS_2 transistors. Nat. Nanotechnol. 2011, 6, 147−150.

[16] F. Bonaccorso, L. Colombo, G. Yu, M. Stoller, V. Tozzini,A. C. Ferrari, R. S. Ruoff, V. Pellegrini, Graphene, related two-dimensional crystals, and hybrid systems for energy conversion and storage; Science 2015, 347, 1246501.

[17] M. Chhowalla, H. S. Shin, G. Eda, L. -J. Li, K. P. Loh, H. Zhang, The chemistry of two-dimensional layered transition metal dichalcogenide nanosheets Nat. Chem. 2013, 5, 263.

[18] M. Chhowalla, Z. Liu, H. Zhang, Chem. Soc. Rev. **2015**, 44, 2584

[19] Côté, A. P.; Benin, A. I.; Ockwig, N. W.; O'Keeffe, M.; Matzger, A. J.; Yaghi, O. M. Porous, Crystalline, Covalent Organic Frameworks ; Science 2005, 310, 1166−1170.

[20] Feng, X.; Ding, X.; Jiang, D. Covalent Organic Frameworks. Chem. Soc. Rev. 2012, 41, 6010−6022.

[21] Diercks, C. S.; Yaghi, O. M. The Atom, the Molecule, and the Covalent Organic Framework. Science 2017, 355, eaal1585.

[22] Covalent organic frameworks: Design principles, synthetic strategies, and diverse applications
Hesham R. Abuzeid, Ahmed F.M. EL-Mahdy , Shiao-Wei Kuo ; Giant, 6, 2021, 100054

[23] Covalent Organic Frameworks: Design, Synthesis, and Functions ; Keyu Geng, Ting He, Ruoyang Liu, Sasanka Dalapati, Ke Tian Tan, Zhongping Li, Shanshan Tao, Yifan Gong, Qiuhong Jiang, and Donglin Jiang Chem. Rev. 2020, 120, 8814−8933

[24] State of the art two-dimensional covalent organic frameworks: Prospects from rational design and reactions to applications for advanced energy storage technologies
Rashid Iqbal, Ghulam Yasin, Mathar Hamza, Shumaila Ibraheem, Bakhtar Ullah, Adil Saleem, Sajjad Ali, Sabir Hussain, Tuan Anh Nguyen, Yassine Slimani, Rajesh Pathak ; Coordination Chemistry Reviews 447 (2021) 214152

[25] Interface-Assisted Synthesis of 2D Materials: Trend and Challenges
Renhao Dong, Tao Zhang, Xinliang Feng
Chem. Rev. 2018, 118, 13, 6189–6235

[26] **a)** Controlling a Chemical Coupling Reaction on a Surface: Tools and Strategies for On-Surface Synthesis
Sylvain Clair, Dimas G. de Oteyza ; Chem. Rev. 2019, 119, 4717−4776; **b**) P. Ruffieux et al., Nature 531, 489 (2016), **c)** Shoatang Son et al. Chem. Soc. Rev., 2021,50, 3238

[27] 2D Covalent Organic Frameworks: From Synthetic Strategies to Advanced Optical-Electrical-Magnetic Functionalities
Congyong Wang, Zhicheng Zhang, Yating Zhu, Chenhuai Yang, Jishan Wu, Wenping Hu
Adv. Mater. 2022, 34, 2102290

[28] Self-assembled one-dimensional carbon nitride architectures ; Jie Li, Chuanbao Cao, Jianwei Hao, Hailin Qiu, Yajie Xu, Hesun Zhu ; Diamond & Related Materials 15 (2006) 1593–1600

[29] Synthesis of Carbon Nitride Nanotubes via a Catalytic-Assembly Solvothermal Route
Chuanbao Cao, Fulin Huang, Chuantang Cao, Jie Li, and Hesun Zhu ; Chem. Mater., Vol. 16, No. 25, p. 5213, 2004

[30] Synthesis and characterization of graphite-like carbon nitride nanobelts and nanotubes
Jie Li, Chuanbao Cao, Hesun Zhu ; Nanotechnology 18 (2007) 115605

[31] Graphitic carbon nitride nanotubes: a new material for emerging applications ; Oleksandr Stroyuk, Oleksandra Raievska, Dietrich R. T. Zahn ; RSC Adv., 2020, 10, 34059

[32] From All-Triazine C_3N_3 Framework to Nitrogen-Doped Carbon Nanotubes: Efficient and Durable Trifunctional Electrocatalysts ; Jian Zeng, Zhongxin Chen, Xiaoxu Zhao, Wei Yu, Shaofei Wu, Jiong Lu, Kian Ping Loh, Jishan Wu ; ACS Appl. Nano Mater. 2019, 2, 7969−7977

[33] Li and Na Co-decorated carbon nitride nanotubes as promising new hydrogen storage media
Yu Sheng Wang, Meng Li, Fei Wang, Qiang Sun, Yu Jia ; Physics Letters A 376 (2012) 631–636

[34] First-principles prediction of an intrinsic half-metallic graphitic hydrogenated carbon nitride ; Huanhuan Qiu, Zhijun Wang, Xianlei Sheng ; Physics Letters A 377 (2013) 347–350

[35] **a)** Advances in Carbon Nitride-Based Materials and Their Electrocatalytic Applications
Farzaneh Besharat, Fatemeh Ahmadpoor, Zahra Nezafat, Mahmoud Nasrollahzadeh, Nilesh R. Manwar, Paolo Fornasiero, Manoj B. Gawande; ACS Catal. 2022, 12, 5605−5660; **b)** Triazine-Based Graphitic Carbon Nitride: a Two-Dimensional Semiconductor; Gerardo Algara-Siller, Nikolai Severin, Samantha Y. Chong, Torbjçrn Bjçrkman, Robert G. Palgrave, Andrea Laybourn, Markus Antonietti, Yaroslav Z. Khimyak, Arkady V. Krasheninnikov, Jorgen P. Rabe, Ute Kaiser, Andrew I. Cooper, Arne Thomas, Michael J. Bojdys, Angew. Chem. Int. Ed. 2014, 53, 7450 –7455; **c)** Ultrathin 2D Graphitic Carbon Nitride on Metal Films: Underpotential Sodium Deposition in Adlayers for Sodium-Ion Batteries;
Lu Chen, Runyu Yan, Martin Oschatz, Lei Jiang, Markus Antonietti, and Kai Xiao; Angew. Chem. Int. Ed. 2020, 59, 9067 – 9073

[36] During the preparation of the manuscript, a related approach was described :
Xunshan Liu, Adam Matej, Tim Kratky, Jesús I. Mendieta-Moreno, Sebastian Günther, Pingo Mutombo, Silvio Decurtins, Ulrich Aschauer, Jascha Repp, Pavel Jelinek, Shi-Xia Liu, Laerte L. Patera ; Angew. Chem. Int. Ed., 2021, doi.org/10.1002/anie.202112798

[37] a) J. D. Lamb, R. M. Izatt, J. J. Christensen, D. J. Eatough ; Coordination Chemistry of Macrocyclic Compounds, ed G.A. Melson, pp. 145-217. Plenum Press, New-York (1979); b) P. Seiler, M. Dobler, J.D. Dunitz ; Acta Cryst., B30, 3744 (1974)

[38] Chemistry of Multitudinous Active Sites for Oxygen Reduction Reaction in Transition Metal − Nitrogen − Carbon Electrocatalysts ; Kateryna Artyushkova, Alexey Serov, Santiago Rojas-Carbonell, Plamen Atanassov
J. Phys. Chem. C 2015, 119, 25917

[39] Molecular spectroscopy by means of ESCA ; Bernt J. Lindbergh, Jan Hedman ; Chemica Scripta, 1975, 7, p . 155

[40] XPS OF NITROGEN-CONTAINING FUNCTIONAL GROUPS ON ACTIVATED CARBON
R. J. J. JANSEN and H. VAN BEKKUM
Carbon Vol. 33, No.8, p. 1021, 1995

[41] Revisiting Nitrogen Species in Covalent Triazine Frameworks; Dmitrii Yu. Osadchii, Alma I. Olivos-Suarez, Anastasiya V. Bavykina, Jorge Gascon; Langmuir 2017, 33, 50, 14278

[42] Diaminotetrazine based mesoporous C3N6 with a well-ordered 3D cubic structure and its excellent photocatalytic performance for hydrogen evolution; Siddulu Naidu Talapaneni, Gurudas P. Mane, Dae-Hwan Park, Kripal S. Lakhi, Kavitha Ramadass, Stalin Joseph, William M. Skinner, Ugo Ravon, Khalid Al-Bahilyb, Ajayan Vinu; J. Mater. Chem. A, 2017, 5, 18183.

[43] Nitrogenated holey two-dimensional structures
J. Mahmood, E. K. Lee, M. Jung, D. Shin, I. Y. Jeon, S. M. Jung, H. J. Choi, J. M. Seo, S. Y. Bae, S. D. Sohn,N. Park, J. H. Oh, H. J. Shin, J.B. Baek, Nat. Commun. 2015, 6, 6486

[44] Versatile, Aqueous Soluble C_2N Quantum Dots with Enriched Active Edges and Oxygenated Groups ; Xuanhe Hu, Linfeng Zhong, Chenhao Shu, Zhengsong Fang, Meijia Yang, Jing Li, ingshan Yu ;J. Am. Chem. Soc. 2020, 142, 4621−4630

[45] **a)** Superior Compatibility of C_2N with Human Red Blood Cell Membranes and the Underlying Mechanism; Lu Liu, Shitong Zhang, Lin Zhao, Zonglin Gu, Guangxin Duan, Bo Zhou, Zaixing Yang, Ruhong Zho; Small 2018, 14, 1803509 ; **b)** Two-dimensional amine and hydroxy functionalized fused aromatic covalent organic framework; Javeed Mahmood, Ishfaq Ahmad, Minbok Jung, Jeong-Min Seo, Soo-Young Yu, Hyuk-Jun Noh, Young Hyun Kim, Hyung-Joon Shin, Jong-Beom Baek; COMMUNICATIONS CHEMISTRY, (2020) 3:31, https://doi.org/10.1038/s42004-020-0278-1; **c)** Recent Progress in Porous Fused Aromatic Networks and Their Applications, Ahmad, I., Mahmood, J., and Baek, J.B. (2020) ; Small Sci. 1, 2000007.

[46] C_2N: A Class of Covalent Frameworks with Unique Properties ; Zhihong Tian, Nieves López-Salas, Chuntai Liu, Tianxi Liu, Markus Antonietti ; Adv. Sci. 2020, 7, 2001767

[47] Y. et al. Tunable C_2N Membrane for High Efficient Water Desalination; Sci. Rep. 6, 29218; doi: 10.1038/srep29218 (2016)

[48] Qu, Y. et al. Highly Efficient Quantum Sieving in Porous Graphene-like Carbon Nitride for Light Isotopes Separation. Sci. Rep. 6, 19952; doi: 10.1038/srep19952 (2016).

[49] Drop-coated C2N electrode for Hydrogen Evolution Reaction
Xiangyu Zhou, Qihao Zhang, Xian-shang Luo, Xu Zhang, Yetong Wu, Yujiu Jiang, Muhua Huang, Tinglu Song, Yanbo, Yang, Junfeng Han;
Materials Letters 309 (2022) 131428

[50] **a)** NbSe2 Meets C2N: A 2D-2D Heterostructure Catalysts as Multifunctional Polysulfide Mediator in Ultra-Long-Life Lithium–Sulfur Batteries

Dawei Yang, Zhifu Liang, Chaoqi Zhang, Jordi Jacas Biendicho, Marc Botifoll, Maria Chiara Spadaro, Qiulin Chen, Mengyao Li, Alberto Ramon, Ahmad Ostovari Moghaddam, Jordi Llorca, Jiaao Wang, Joan Ramon Morante, Jordi Arbiol, Shu-Lei Chou, and Andreu Cabot; Adv. Energy Mater. 2021, 11, 2101250; **b)** An efficient and pH-universal ruthenium-based catalyst for the hydrogen evolution reaction; Javeed Mahmood, Feng Li, Sun-Min Jung, Mahmut Sait Okyay, Ishfaq Ahmad, Seok-Jin Kim, Noejung Park, Hu Young Jeong3, Jong-Beom Baek; Nature Nanotech 12, 441–446 (2017); **c)** J. Mahmood, F. Li, C. Kim, H.-J. Choi, O. Gwon, S.-M. Jung, J.-M. Seo, S.-J. Cho, Y.-W. Ju, H. Y. Jeong, G. Kim, J.-B. Baek, Nano Energy 2018, 44, 304

[51] Molten salt assisted pyrolysis approach for the synthesis of nitrogen-rich microporous carbon nanosheets and its application as gas capture sorbent ; Miao Zhang, Lin Liu, Teng He, Xiaohua Ju, Ping Chen ; Microporous and Mesoporous Materials 300 (2020) 110177

[52] Template- and Metal-Free Synthesis of Nitrogen-Rich Nanoporous "Noble" Carbon Materials by Direct Pyrolysis of a Preorganized Hexaazatriphenylene Precursor; Ralf Walczak, Bogdan Kurpil, Aleksandr Savateev,Tobias Heil, Johannes Schmidt, Qing Qin, Markus Antonietti, Martin Oschatz; Angew.Chem. Int. Ed. 2018, 57,10765–10770

[53] Polarized light microscopy of chemicalvapor-deposition-grown graphene on copper ; K. Kertész, A. A. Koós, A. T. Murdock, et al. ; Appl. Phys. Lett. 100, 213103 (2012)

[54] Large cross-polarization rotation of light on graphene; Jian Liu, Shizhen Chen, Hailu Luo, et al; Appl. Phys. Lett. 119, 081104 (2021)

[55] Protonation-Assisted Exfoliation of N-Containing 2D Conjugated Polymers : Xinlei Zhang, Xiao Luo, Xusheng Zheng, Xiaojun Wu, Hangxun Xu ; Small 2019, 15, 1903643

[56] Imaging Beam-Sensitive Materials by Electron Microscopy
Qiaoli Chen, Christian Dwyer, Guan Sheng, Chongzhi Zhu, Xiaonian Li, Changlin Zheng, Yihan Zhu;
Adv. Mater. 2020, 32, 1907619

[57] Stacking stability of C2N bilayer nanosheet
Klichchupong Dabsamut, Jiraroj T-Thienprasert, Sirichok Jungthawan, Adisak Boonchun;
Scientific Reports (2019) 9:6861 ; https://doi.org/10.1038/s41598-019-43363-8

58 Graphitic carbon nitride materials: variation of structure and morphology and their use as metal-free catalysts; Arne Thomas, Anna Fischer, Frederic Goettmann, Markus Antonietti, Jens-Oliver Müller, Robert Schlögl, Johan M. Carlsson J. Mater. Chem., 2008, 18, 4893–4908

[59] Tian Sun, Yan Liang, and Yuxi Xu, Angew. Chem. Int. Ed. 2021, 60, doi.org/10.1002/anie.202113926

[60] Kewei Wang, Li-Ming Yang, Xi Wang, Liping Guo, Guang Cheng, Chun Zhang, Shangbin Jin, Bien Tan, Andrew Cooper; Angew. Chem. Int. Ed. 2017, 56, 14149 –14153

[61] Siquan Zhang, Guang Cheng, Liping Guo, Ning Wang, Bien Tan, Shangbin Jin; Angew Chem Int Ed Engl. 2020, 59(15): 6007

[62] **a)** Hayami, S.; Inoue, K., Chem. Lett., (1999), 545 ; **b)** Heteroarenes and related ring systems, von Angerer, S., Science of Synthesis, (2004) 17, 475. DOI: 10.1055/sos-SD-017-00728

[63] Controllable and Large-Scale Synthesis of Carbon Nanostructures: A Review on Bamboo-Like Nanotubes; Zirui Jia, Kaichang Kou, Ming Qin, Hongjing Wu, Fabrizio Puleo, Leonarda Francesca Liotta; Catalysts 2017, 7, 256; doi:10.3390/catal7090256

[64] Characterization of graphene nanosheets obtained by a modified Hummer's method; Renata Hack, Cláudia Hack Gumz Correia, Ricardo Antônio de Simone Zanon, Sérgio Henrique Pezzin; Artigo • Matéria (Rio J.) 23 (1) • 2018 • https://doi.org/10.1590/S1517-707620170001.0324